LUND UNIVERSITY

Patterning of perovskite thin films for electrical and optical characterisation

Nils Lamers

Thesis submitted for the degree of Master of Science
Duration: 9 months

Supervised by Prof. Magnus Borgström and Dr. Michael Winters

Department of Physics
Division of Solid State Physics
June 2020

Abstract

While perovskite solar cells have become increasingly more efficient and popular, electrical characterisation of the semiconductor properties of perovskites has been limited due to the instability of the material. In this work, multiple approaches for creating such electrical test structures from perovskites are discussed. The chemical processing limitations for perovskites are laid out and common semiconductor processes are discussed from the viewpoint of perovskite compatibility. A partially successful spin-on patterning approach is demonstrated by combining a patterned silane-based hydrophobic layer with liquid phase perovskite deposition. Structured perovskite is successfully created with a top-down approach by lithographic patterning of a perovskite compatible resist stack and pattern transfer via ion beam etching. Photoluminescence measurements are used to confirm that the perovskite remained unaffected by the patterning process. Patterning of the contact layer and successful deposition of a CuSCN transport layer using deep-UV lithography are shown. An alternative approach using electron beam lithography is discussed.

Popular science abstract

Research into clean energy technologies has become increasingly more important over the last few decades, spurned by growing popular demand and fear of climate change. As silicon solar cells approach their theoretical efficiency limit, emerging technologies may hold the key to even more efficient solar cells. One such technology is that of perovskite solar cells, which have risen from 3.8% efficiency to 25.2% in just a decade. Additionally, perovskites can be processed from a liquid phase, allowing for large scale processing methods like those used for plastics. This makes production significantly cheaper when compared to conventional solar cells. However, their high solubility also makes perovskites difficult to process, which has so far limited study of their electrical properties and limited integration with other technologies. In order to study semiconductors and create functional devices, the materials need to be patterned. That is, the shape of the material needs to be under direct control of the researcher so that the semiconductor conforms to the shape required for the experiment. This microscopic patterning of perovskites has proven difficult, as patterning methods were primarily developed for more stable semiconductors like silicon. When using these methods to pattern perovskites, they will generally be damaged during the processing. In order to achieve the microscopic patterning necessary to study the semiconductor properties of perovskites, new processing methods must be created. The processing methods discussed in this thesis allow for the creation of such microscopic perovskite devices. Furthermore, understanding obtained from these devices can then be applied to further increase the efficiency of perovskite solar cells, while the processing methods can be used to integrate perovskites with already existing semiconductor technologies.

Acronyms

DI water	deionised water
DMF	dimethylformamide
DMSO	dimethyl sulfoxide
DPGDME	dipropylene glycol dimethyl ether
DUV	deep UV
EBL	electron beam lithography
ETL	electron transport layer
FA	formamide
HSQ	hydrogen silsesquioxane
HTL	hole transport layer
HZB	Helmholtz-Zentrum Berlin
IBE	ion beam etching
ITO	indium tin oxide
IPA	isopropylalcohol
LNL	Lund Nano Lab
LOR	lift-off resist
MA	methylammonium
MIBK	methyl isobutyl ketone
NMP	N-methyl-2-pyrrolidone
ODTS	octadecyltrichlorosilane
P3HT	poly(3-hexylthiophene)
PCBM	phenyl-C61-butyric acid methyl ester
PEDOT	poly(3,4-ethylenedioxythiophene)
PFOTS	perfluorooctyltrichlorosilane
PGME	propylene glycol methyl ether
PGMEA	propylene glycol methyl ether acetate

PL	photoluminescence
PMMA	poly(methyl methacrylate)
PSK	perovskite
PSS	polystyrene sulfonate
PTAA	poly tri-arylamine
poly-TPD	poly(4-butylphenyldiphenylamine)
RIE	reactive ion etching
SAM	self-assembled monolayer
SEM	scanning electron microscopy
spiro-OMeTAD	2,2,7,7-tetrakis[N,N-di(4-methoxyphenyl)amino]-9,9-spirobifluorene
TDL	top-down lithography
TMAH	tetramethylammonium hydroxide

Contents

1. Introduction

1.1. Motivation

As a result of an increasing global research effort into renewable energy technologies, the field of perovskite solar devices has grown significantly over the last 10 years [1, 2]. With a rise in efficiency from 3.8% to 25.2% in just a decade [3], perovskite solar devices have improved at a faster rate than any other solar technology. This promise of excellent performance is combined with the ability to process devices from solution, allowing for inexpensive and simple processing when compared to other solar cell technologies [1, 2].

However, as perovskite solar cell technology has advanced, little research has been undertaken into the semiconductor properties of perovskites. Notably, directly probing the material using electrical measurements to determine charge carrier properties has been neglected due to a lack of established perovskite processing techniques. While perovskite solar cells perform well despite this gap of knowledge, understanding the semiconductor properties of perovskites may unlock further theoretical and practical tools for improving perovskite solar cells. Additionally, these new processing methods may facilitate the use of perovskites in other fields of research.

Currently, perovskite properties are mostly explored using optical methods such as photo-luminescence spectroscopy and by measuring the electrical properties of perovskite solar cells [4]. Since perovskite solar cells are effectively two-terminal photodiodes, very little information about the perovskite can be obtained. More intricate measurements such as Hall effect measurements are required in order to obtain properties like charge

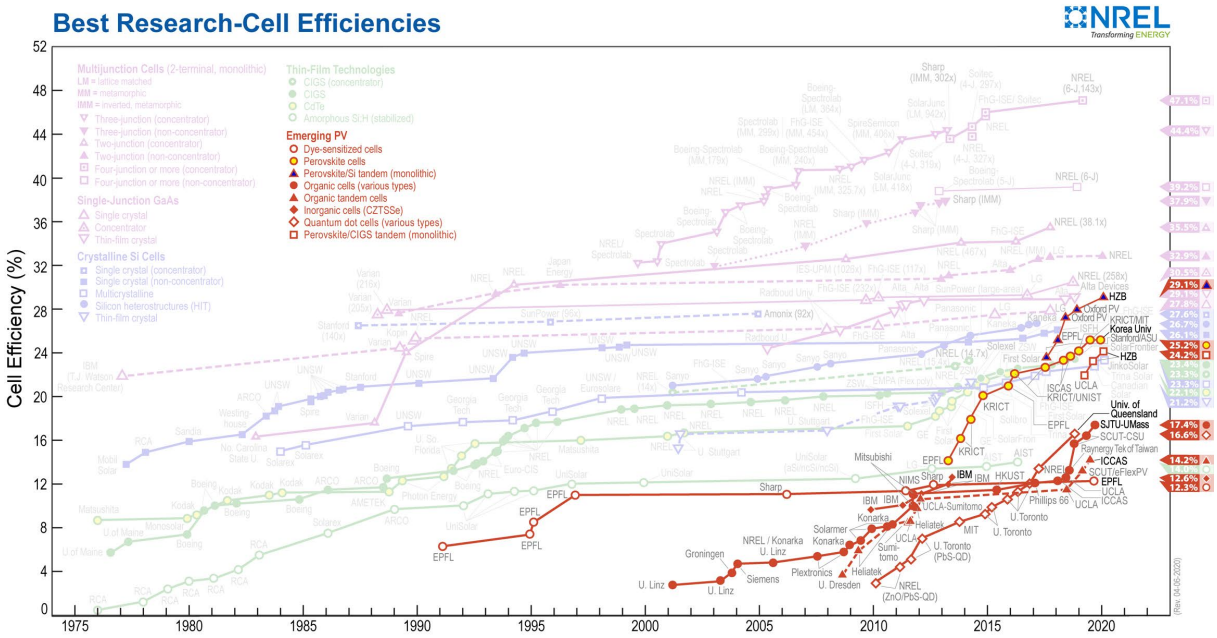

Figure 1: Development of top efficiency for lab-scale perovskite solar devices [3].

carrier mobility. These measurements require more intricate processing, with patterning control over the structure of the perovskite and over the structure of the contacts being necessary.

This is where the solubility of perovskites which allows for solution-processing proves to be disadvantageous. While solution processing trivialises creating planar perovskite films for solar cells via spin-coating, perovskites will dissolve in most processing chemicals required for lithographic patterning. Overcoming this challenge and mastering perovskite patterning is key to constructing more advanced electronic devices from perovskites. Viable process technologies are also required to integrate perovskites with other technologies, like the nanowire-perovskite tandem solar cells currently being developed at Lund Nano Lab (LNL). This thesis discusses the development of a processing scheme for patterning and contacting perovskite device for Hall effect measurements and other electrical measurements.

1.2. Scientific background

1.2.1. Perovskite thin films

The foundation of perovskite solar cell technology are perovskite thin films. Perovskites are a group of materials all of which conform to a common crystal structure and the general chemical formula ABX_3. In this formula, A^+ is a cation, B^{2+} is the coordinating ion, and X^- is the anion. Structurally, the unit cell of the material is as shown in Figure 2 with the A^+ cation on the corners, the B^{2+} cation in the centre, and the X^- anions on the faces [2]. This structure and formula are generic to all perovskites, but the chemical compositions of perovskites and their resulting physical properties vary quite significantly. The perovskites studied as semiconductors for solar applications are mostly lead-halide perovskites (henceforth simply called perovskites), with the B^{2+} cation being lead Pb^{2+} and the X^- anion being a halide (Cl^-, Br^-, I^-)[1]. Three different A^+ cations are the focus of research. These are the formamide (FA) cation CH_3NO^+, the methylammonium (MA) cation $CH_3NH_3{}^+$, the caesium cation (Cs^+).

The chemical compositions of the perovskites are a significant focus of energy research. Perovskites are often prepared using multiple elements as for A^+ cations (e.g. $A^+ = Cs_{0.5}$, $MA_{0.5}$) or X^- (e.g. $X^- = Br_{0.5}, I_{0.5}$) anions. Different compositions result in different band gaps and electrical properties, which tunes the behaviour of the resulting solar cell. The coordinating ion is typically $Pb_2{}^+$, but experimental perovskites using tin $Sn_2{}^+$ have also been prepared. Although the detailed physical properties vary between these different perovskite compositions, the photoactive and semiconductor behaviour is common to lead-halide perovskites [2].

Notably, perovskites have a very low enthalpy of formation [2], meaning it is energetically cheap to create perovskite material from precursor materials. As a result, perovskites can be processed at room temperature from precursor solutions containing reactants. These solutions consist of lead-halide salts (e.g. $PbBr_2$, PbI_2, etc.) and halide-cation salts (e.g. CsBr, MAI, etc.) dissolved in polar organic solvents like dimethylformamide (DMF) or dimethyl sulfoxide (DMSO). The liquid-phase processing of perovskites allows for the use varied and scalable processing techniques such as roll-to-roll or slot-die printing [2].

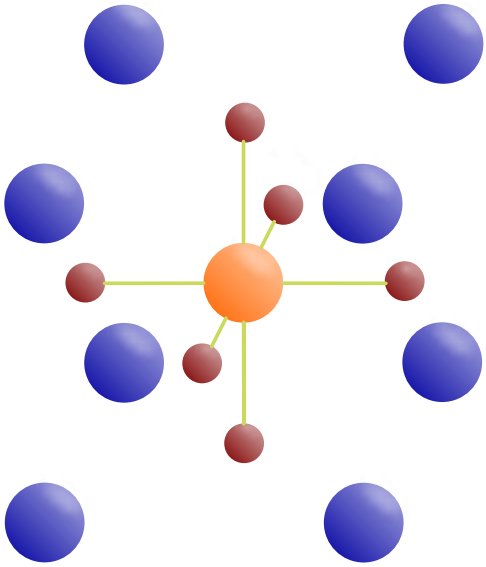

Figure 2: Unit cell of perovskite. The blue corner atoms are A^+ cations, the orange central atom is a B^{2+} cation and the red face atoms are X^- anions.

When prepared for research purposes, perovskite thin films are generally deposited from liquid precursors by a process called spincoating, as discussed below.

1.2.2. Spincoating of thin films

Spincoating is a processing method that allows for the creation thin films of uniform thickness from liquid solutions. It is commonly employed for deposition of perovskite thin films but is also a staple processing method for the deposition any thin film from solution.

To deposit a thin film using spincoating, the substrate is first placed onto a spincoating chuck. Using a hole in the centre of the chuck the substrate can be secured by applying vacuum suction. The liquid containing the thin film chemical is then pipetted onto the substrate until the entire surface is covered but before the surface tension of the liquid breaks. The spincoater can then be started, which will rotate the chuck. The resulting centrifugal force forces some of the liquid away from the centre and off the edge of the substrate. This leaves a thin film of uniform height on the substrate, with slightly thicker film at the edge, as a result of liquid building up there. The experimental setup for spincoating is illustrated in Figure 3. At the end of the spinning process, the sample is placed on a hot plate. This quickly evaporates any remaining solvent from the sample surface and leaves behind the desired thin film.

The height of the liquid H as it evolves during spincoating can be described by Equation 1 [5], with initial liquid height h_0, spin speed ω, spin time t, liquid viscosity η, and liquid density ρ.

$$H = h_0 \left(1 + \frac{4h_0^2 \rho w^2 t}{3\eta}\right)^{-\frac{1}{2}} \tag{1}$$

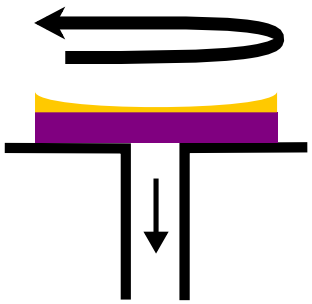

Figure 3: Schematic of the spincoating process. The substrate is fixed to the chuck via vacuum suction while the liquid is forced off of the substrate by centrifugal forces.

Spin speeds ω are typically in the area of 1000 rpm to 6000 rpm and spin times t are generally kept between 30 s to 60 s so that not all the solvent has evaporated prior to placing the sample on the hot plate. The data sheets for commercially sold polymer solutions generally contain spin curves, which show the film thickness obtained for given spin speeds and spin time. For self-prepared solutions, these spincurves need to be obtained experimentally.

1.2.3. Lithographic processing and patterning

Reliable and accurate measurement techniques for assessing semiconductor material parameters have been developed over the last fifty years. These techniques generally require the semiconductor material to be processed into specific test structures with a designated shape for both the semiconductor material and the contact material(s). These test structures are generally manufactured on a microscopic or sub-micrometre scale, which maximises the devices per sample area and allows the studying of quantum effects. This small scale processing is made possible only by sophisticated processing methods, chief among which is lithography.

Lithography is based around the patterning of a substitute layer, called lithography resist, on top of the active sample layer. The pattern imparted onto this layer can then by transferred into the active sample layers by etching or can be inherited by a newly deposited layer of the sample. After patterning, the lithography layer is typically removed, leaving behind only an active patterned structure. Two key lithography techniques are photolithography and electron beam lithography (EBL), as discussed below.

Photolithography uses UV light to transfer a pattern from a photomask to a layer of light-sensitive photoresist. Photoresists are generally organic polymers and epoxies that are designed to change their chemical structure when exposed to light. To achieve lithographic patterning, a uniform layer of photoresist is first deposited onto the sample surface using spincoating. The resist is then cured thermally to remove any solvents. The sample is then exposed to patterned UV light and patterning is achieved by placing a photomask between the light source and sample surface. Onto the photomask, the master pattern is printed in metal, which shadows the master pattern onto the sample surface, exposing only select areas to light. To properly align the light source, photomask,

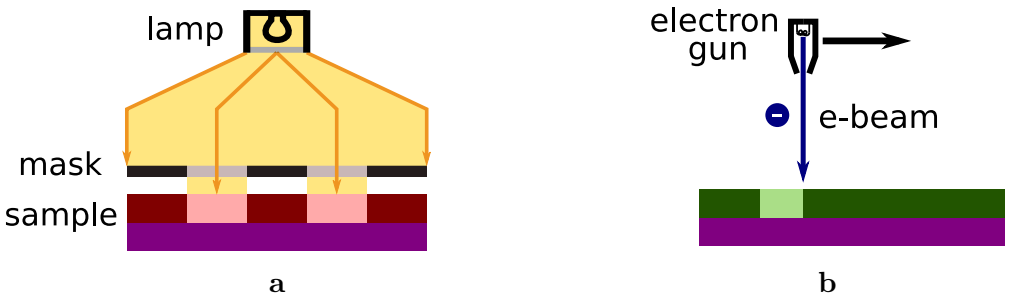

Figure 4: Illustrations of the exposure processes for photolithography and EBL. a) Photolithography exposure with unexposed photoresist (■) and exposed photoresist (■). The entire sample can be exposed at once. b) EBL exposure with unexposed photoresist (■) and exposed photoresist (■). The electron beam moves over each spot that is to be exposed.

and sample surface on a microscopic scale, a device called a mask aligner is used. A photolithographic exposure is illustrated in Figure 4a.

In the areas exposed to UV light, the light-sensitive components of the photoresist are chemically activated. The subsequent reaction leads to a chemical difference between exposed and unexposed areas of photoresist. Sometimes, this reaction needs to be enhanced by introducing thermal energy to the sample in what is called a post-exposure bake.

The sample is then placed into a solvent which will selectively dissolve either exposed or unexposed areas of resist. This process is called development and the solvent is referred to as a developer. If the exposed areas of photoresist are removed by the developer, then the photoresist is said to have positive tone. If the unexposed areas are removed, it is said to have negative tone. After development, a patterned layer of resist remains on the sample.

EBL works by the same principle as photolithography, but instead of being sensitive to light, the resists are sensitive to high energy electrons. EBL resists also come in positive and negative tones. The exposure process during EBL is vastly different, requiring more time and much more complicated tool. Because the mean free path of electrons outside vacuum is incredibly short, EBL exposure takes place in a vacuum environment and cannot use a physical mask. Instead, the pattern is written onto the sample surface with a focused electron beam and the mask is a software map which tells the tool where to move the beam. An EBL exposure is illustrated in Figure 4b. After EBL exposure, the resist developed and remains behind patterned.

With a layer of patterned resist on the sample, this pattern can be transferred to the active device layers. This is generally done by either etching away the exposed layers of the sample surface or by depositing new material onto these exposed areas. If the sample is to be etched, it can be done by using a directional method of etching such as reactive ion etching (RIE) or ion beam etching (IBE) or using chemically selective but isotropic wet etching. Depositing new material is commonly done for metal layers, such as contacts. The metal is evaporated and deposits onto the sample by diffusing, covering both resist surface and exposed sample surface in a uniform layer. Patterning is then ultimately achieved by dissolving the resist layer, removing both the resist and any metal on top of it from the sample. In the areas exposed during development, the metal will

remain on the sample surface. This step is commonly called a lift-off process.

Both UV photolithography and EBL allow for patterning of semiconductor materials on micrometre and sub-micrometre scales. However, each technique has its advantages and disadvantages. Photolithography is much faster and allows for an area exposure. In contrast, EBL requires loading the sample into a vacuum environment and the passing of a focused electron beam over each area that is to be exposed. While this greatly increases exposure times, it allows EBL to write much smaller features than UV lithography, since the resolution of UV lithography is limited by the wavelength of the UV light used. Another major advantage of EBL is the nature of the mask. While both EBL and photolithography masks can be created using the same software, a photomask needs to be created physically while an EBL mask is just a software file. This means that EBL masks can be changed at no cost and within a matter of minutes.

Patterning of semiconductor material achieved through lithography followed by pattern transfer methods like etching is referred to as top-down patterning.

1.2.4. Ion-beam etching

Ion beam etching (IBE) is a process that etches a surface through physical ablation. During IBE inert ions (commonly argon ion Ar^+) are accelerated towards the target surface where they collide with the atoms that make up the surface. This physically kicks atoms out of the surface material, etching the material. This process is also often called argon milling. Due to the physical nature of the process, it etches all materials, though different materials are etched at different rates. In contrast to reactive ion etching, there are no chemical reactions involved. As a result, IBE does not chemically affect the sample, which makes it suitable for use with more reactive and unstable materials.

1.2.5. Self-patterned deposition

Self-patterned deposition has been demonstrated as an alternative to top-down patterning for perovskites [6, 7]. This process utilises the liquid-phase deposition of perovskites by patterning a hydrophobic material on the substrate before perovskite spincoating. During the spincoating process, the perovskite precursor will more easily adhere to the hydrophilic areas of the substrate, while spinning off of the hydrophobic areas. This results in the perovskite exclusively forming on the hydrophilic substrate. The concept of the process is illustrated in Figure 5.

The theory principles involved in patterned deposition have been extensively discussed by Lee et. al. [7]. In a simplified 2D model, dewetting occurs as the height of the solution on the sample reaches a critical height H_{crit}, dependent on the hydrophilic contact angle θ, the hydrophilic region length L_{phil}, the hydrophobic contact angle β, and the hydrophobic region length L_{phobic} [7]. The relationship is given below in Equation 2.

$$H_{crit} = \frac{(1 - \cos\beta)L_{phobic} + \frac{1}{3}\theta^2 L_{phil}}{2\theta} \tag{2}$$

By equating Equation 2 and Equation 1, the necessary spin speed for a given time and solution can be modelled.

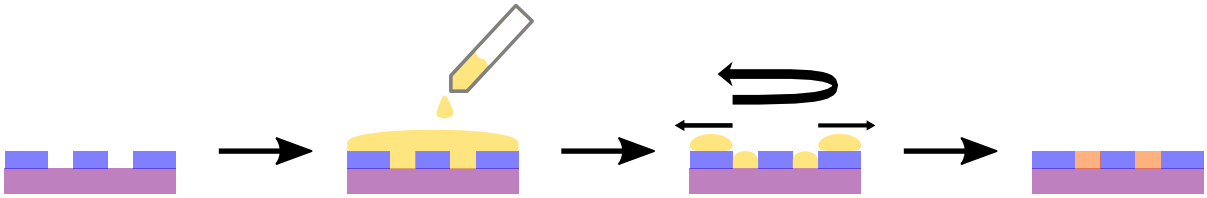

Figure 5: Illustration of the principle of patterned deposition. A hydrophobic layer is patterned (■) onto the substrate (■). During spincoating, the perovskite precursor (■) adheres to the substrate but does not adhere to the hydrophobic layer. This results in the crystallisation of a patterned perovskite film (■).

1.2.6. Transport materials for perovskites

When contacting perovskites devices, carrier selective contacts are commonly employed along the interface between metal contact leads and perovskite material. These materials allow for more efficient carrier extraction due to their band matching with the perovskite [8, 9]. The engineering and optimisation of contact materials is a major part of pervoskite solar cell research.

An electron transport layer (ETL) is chosen so that the conduction band edge of the perovskite and the ETL are suitably aligned so that little change in carrier energy is required for an electron in the perovskite conduction band to move to the ETL conduction band. At the same time, the valence band edges of perovskite and ETL are suitably misaligned, so that it is less favourable for a hole carrier to move from the perovskite into the electron transport layer. Hole transport layers (HTLs) work the opposite way, with the valence band edges being aligned to the perovskite, allowing for good hole carrier extraction, but the conduction band edges being misaligned. Plain metal contacts could be used, but because their band edges typically align poorly with those of the perovskite material, the resulting charge carrier extraction is suboptimal. This is schematically illustrated in Figure 6.

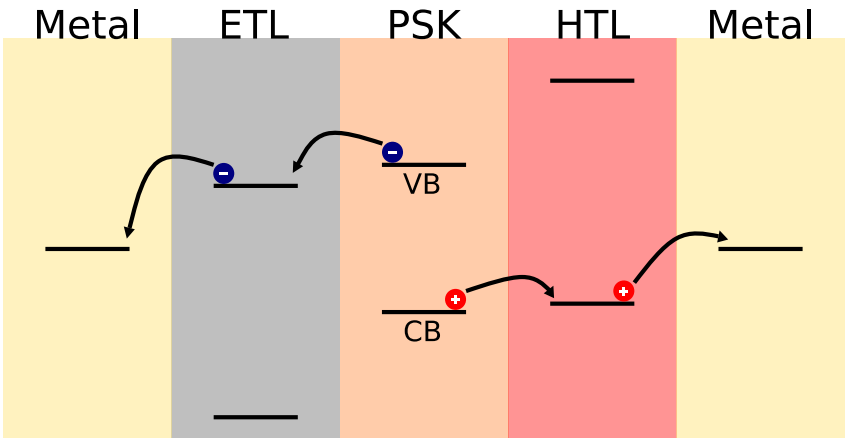

Figure 6: Diagram illustrating band alignment of perovskite (PSK) and selective carrier contacts in a perovskite solar cell. Band positions are not to scale and simply schematic.

1.2.7. Photoluminescence spectroscopy

Photoluminescence (PL) is the emission of light from a sample subsequent to excitation by electromagnetic radiation. When excited by photons with an energy ($\hbar\omega$) larger than the band gap of the material, electrons are promoted from the valence band into the conduction band. These excited electrons can then fall back from the conduction band into the valence band, during which they release the energy difference as a photon. Although electrons could fall from any conduction band level to any empty valence band level, only the transition from conduction band edge to valence band edge are typically seen [10]. By analysing the emitted spectrum, information about electronic structure and composition of the material can be obtained.

1.3. Research strategy

The aim of this work is the development of processing techniques which facilitate the creation of electronic test structures that enable characterisation of the semiconductor properties of perovskites. Three device structures were chosen for fabrication:

- van-der-Pauw squares
- Hall bars
- transmission lines

These device structures allow for basic semiconductor characterisation measurements which give access to a semiconductors carrier properties, resistivity, and the quality of the contacts [11, 12]. The lithography masks required to create these structures are shown in Figure 7. The lithography masks were designed in Tanner L-Edit. Each device consists of a bottom layer of perovskite (orange) onto which contacts are patterned. The contacts consist of a layer of transport material (black) and metal leads (blue) that become contact pads to which measurement devices can be connected. Figure 7a shows the devices structure for van-der-Pauw measurements, Figure 7b the device structure for Hall effect measurements, and Figure 7c the device structure for transmission line measurements. Van-der-Pauw squares were designed for perovskite devices measuring 100 µm by 100 µm and 50 µm by 50 µm. Hall bars were designed for both 50 µm by 100 µm and 100 µm by 200 µm devices.

The goal is to create these three device structures on the same sample, by first patterning a layer of perovskite material, followed by the application of patterned contacts. The fabrication of patterned perovskite presents the larger challenge of the two. This is a consequence of the general lack of perovskite patterning experience within the field and the sensitive nature of the material. Both, a self-patterned and a top-down approach to perovskite patterning are explored. Following successful patterning, photoluminescence measurements are used to confirm that the perovskite material is unaffected. Contact patterning is attempted using top-down lithography, followed by contact material application and lift-off.

This project was conducted in collaboration with Helmholtz-Zentrum Berlin (HZB) in Germany, where perovskite energy materials are a main focus of research.

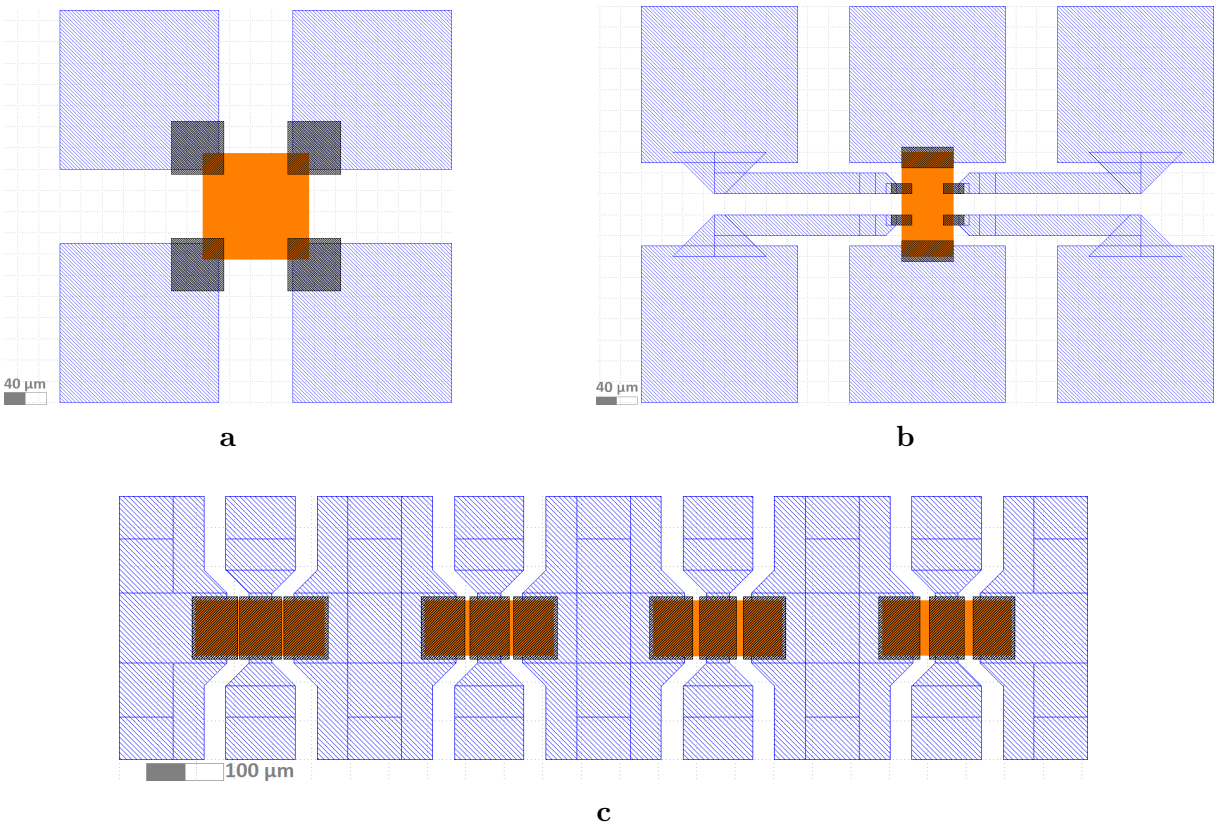

a **b**

c

Figure 7: Images of the designed device and contact structure, showing the three device types present on the sample. Different colours denote different layers of the device: ■ perovskite, ■ carrier transport material, ■ metal contact leads. a) Layout of a 100 µm by 100 µm van-der-Pauw square. b) Layout of a 50 µm by 100 µm Hall bar. c) Layout of a transmission line device.

2. Methods

The compositions of the perovskites used during the thesis are discussed in section 2.1. Since perovskites are easily soluble and chemically vulnerable materials [2, 13], conventional methods of semiconductor processing can typically not be applied to them. The limitations put on solvent selection and processing tools compatible with perovskites are described in section 2.2. These limitations were kept in mind throughout the entire process development for the thesis.

2.1. Perovskite material

Two different perovskites were used throughout the thesis: a triple-cation perovskite, consisting of formamide (FA = CH_3NO), methylammonium (MA = CH_3NH_3), caesium (Cs), and lead (Pb) as cations, and iodine (I) as the anion and more simple CsPbBr. In the structure portrayed in Figure 2 the blue corner atoms correspond the interchangeable FA, MA, or Cs cations, the orange atom in the centre to the Pb cation, and the I anions to the red atoms on the faces.

The triple-cation perovskite was produced at HZB. The precursor solution is spin-coated at 4000 rpm and the sample is then heated on a hot plate at 100 °C for 30 min to evaporate the DMF solvent. Optical images of the pristine perovskite surface are shown in Figure 8. It can be seen that the perovskite includes very few pinholes and other macroscopic defects. In Figure 8b the surface structure of the film is visible, showing clearly that the surface of the perovskite is not completely flat.

$CsPbBr_3$ perovskite was also used to test some processing but not intended for use in final devices. This perovskite was created at chemical physics in Lund.

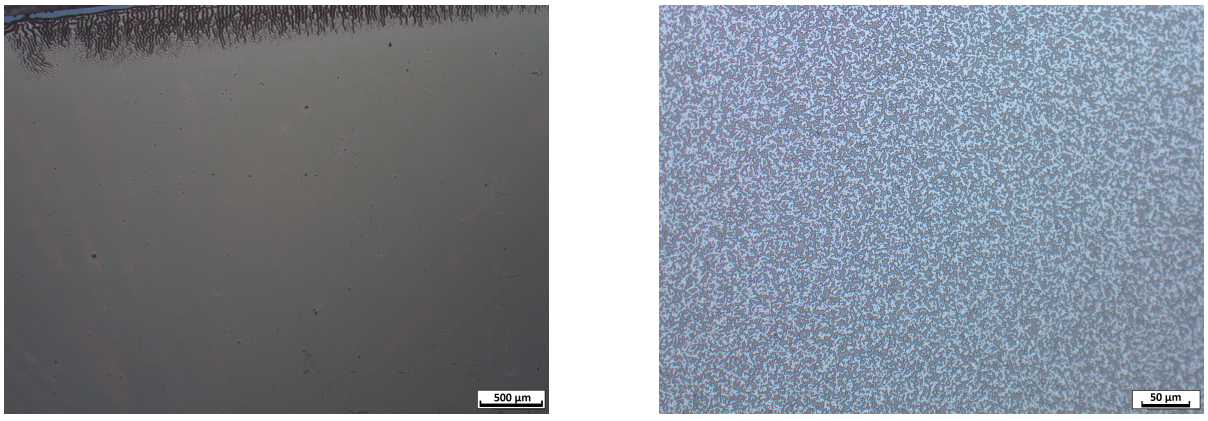

a **b**

Figure 8: Optical images of pristine perovskite films produced at HZB. a) Pristine perovskite surface. b) A closer look at the surface structure of pristine perovskite.

2.2. Processing limits

The instability of perovskite materials places restrictions on processing that must abided by or the perovskite will be destroyed or altered during the processing [2, 13]. Discounting reactions with other chemicals, perovskites face degradation through three mechanisms: dissolution, thermal degradation, and photodegradation [2, 14, 15].

Of these limitations, the high solubility of perovskites is the most difficult to accommodate. Commonly, deionised water (DI water), isopropylalcohol (IPA), and acetone are used as solvents when working with semiconductors. However, these and other polar solvents are capable of dissolving perovskites (or constituent salts) and can therefore not be employed when patterning perovskite test structures. Instead, non-polar solvents that are known to be compatible with perovskites must be used throughout the entire process. Based on solvent tests conducted in literature, these solvents include [1, 7, 16–19]:

- chlorobenzene [17]
- hexane [17, 19]
- toluene [7, 18]
- propylene glycol methyl ether acetate (PGMEA) [19]
- anisole [16]

Temperatures above 200 °C need to be avoided if the perovskite is to remain in the same crystal structure and chemical composition [14]. This limitation is mostly significant for the processing of contact materials, as processes like thermal annealing and thermally intensive deposition methods cannot be applied.

Photodegradation can be limited by storing the samples in a dark environment and avoiding photolithography on perovskites whenever possible.

As lead is a major constituent of perovskites, lead contamination presents a risk during handling. Avoiding any process or chemical that may attack the perovskite is therefore important to maintaining lab safety, as (lead) salts may otherwise be leached out of the sample. Due to the small amounts of perovskite used in the samples, the health risk is negligible [20], but contamination of tools is still a risk. Safe processing of perovskites is integral to maintaining user safety and lab integrity.

3. Results

Two approaches to patterning perovskite were attempted based on published experimental methods [6, 7, 16]. The two approaches are bottom-up patterning approaches using patterned deposition, as discussed in section 3.1, and an approach uses top-down patterning. The choice of available lithography systems as well as a perovskite-compatible multilayer resist system are discussed in section 3.2.

The contacting process for perovskite devices is universal to all patterning approaches. but still requires adjustments relative to standard processing techniques. The considerations and choices for transport layers as well as lithographic processing for contacting are described in section 3.3.

3.1. Self-patterned deposition

As a first step, self-patterned deposition (Figure 5) was attempted because it offers multiple advantages over standard top-down processing. For instance, the methods that can be used to pattern the hydrophobic layers before perovskite deposition are far less limited, when compared to the methods available for direct patterning of perovskite. Additionally, the time between perovskite deposition and creation of the finished device is shortened, which minimises the degradation of perovskite at point of measurement.

3.1.1. Self-patterned deposition using poly-TPD layer

Spin-on patterning was attempted using a poly(4-butylphenyldiphenylamine) (poly-TPD) polymer layer, as demonstrated by Wu et. al. [6]. Since it is soluble in chlorobenzene, poly-TPD can be removed after successful spin-coating without affecting the perovskite.

Poly-TPD was purchased from Sigma-Aldrich and solutions containing $10\,\mathrm{mg\,ml^{-1}}$ and $20\,\mathrm{mg\,ml^{-1}}$ in chlorobenzene (also obtained from Sigma-Aldrich) were prepared for spincoating. Spin curves for both solutions were created by spinning them onto cleaned SiO_2 substrates for 60 s at varying speeds. The thickness of the films was measured using a Bruker Dektak profilometer. The resulting thicknesses and spincurves are plotted in Figure 9 with the spincurves fitted for a time-thickness relationship (Equation 1). It should be noted that neither solution produced a uniform thin film for spin speeds below 3000 rpm.

The SiO_2 substrates were cleaned in acetone and IPA using an ultrasonic cleaner, after which $20\,\mathrm{mg\,ml^{-1}}$ poly-TPD solution was spincoated at 3000 rpm for 30 s resulting in a $\approx 55\,\mathrm{nm}$ thick film. These spincoating parameters were chosen because they offered the largest thickness while still creating a uniform layer. The samples were then heated on a hotplate at 120 °C for 120 s to remove the remaining chlorobenzene. Afterwards, AZ1505 photoresist from MicroChemicals was spun on at 4000 rpm for a 500 nm thick film, before being cured on a hotplate at 100 °C for 50 s. The photoresist was then exposed using a Süss MJB4 soft UV mask aligner with a dose of $200\,\mathrm{mJ\,cm^{-2}}$ before being developed in AZ351B developer (1:5 dilution with DI water) for 30 s and washed in DI water. Samples were then spin-drop cast with chlorobenzene to transfer the pattern from the photoresist into the poly-TPD layer. In this process samples were fixed on the spincoater and multiple drops of chlorobenzene were pipetted onto them without breaking surface tension. After 12 s the chlorobenzene had dissolved the underlying poly-TPD and the samples were spun at 3000 rpm for 30 s to remove the chlorobenzene. Following pattern transfer, the samples were placed on a 120 °C hot plate to remove the remaining chlorobenzene. Since the resulting pattern transfer was imperfect with small flakes of poly-TPD left behind, the samples were also etched via RIE (40 sccm O_2, 10 sccm Ar, 100 mTorr, 100 W, 40 s). Afterwards the AZ1505 was removed by immersion in acetone and rinse in IPA. The progress of the sample throughout the process steps is shown in Figure 10.

To confirm that the poly-TPD layer is hydrophobic, surface angle measurements were conducted using a Theta Lite tensiometer and DI water at LNL. Water was used instead of perovskite precursor, as the samples were to be spincoated at HZB and perovskite precursor solution was not available at LNL at the time. The contact angle for DI water

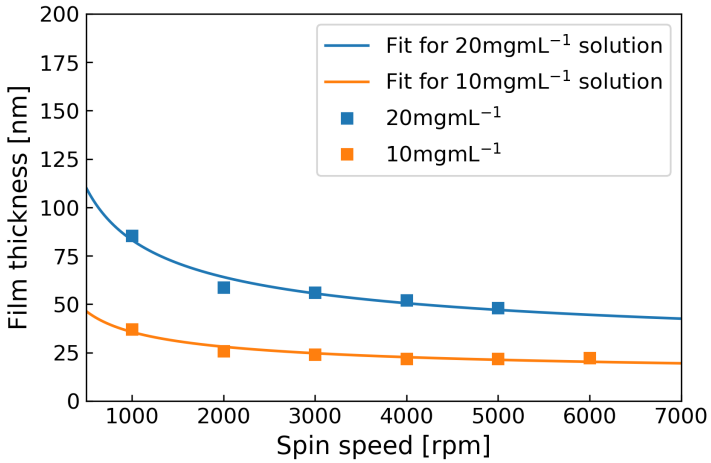

Figure 9: Spin curves obtained for 10 mg ml^{-1} and 20 mg ml^{-1} solutions of poly-TPD in chlorobenzene. Spin curves were fitted for Equation 1.

on a poly-TPD film prepared as above was measured to be 89°. The contact angle on the same SiO_2 sections of the same samples was measured to be 49°. This means that the poly-TPD films show a hydrophobic nature, although it is not as pronounced as with more specialised coatings. Using Equation 1 and Equation 2, the necessary spin speed (for $t = 60$ s) to achieve dewetting of water can be calculated, as described in Appendix A. The patterned samples were sent to HZB for spincoating, but even at spin speeds of 6000 rpm no dewetting was observed. Instead, the samples were fully covered in a perovskite film. This can be explained by the level of hydrophobicity exhibited by poly-TPD layers. Contact angles for water are sufficient for dewetting, but only at high speeds. Should the precursor be less polar or have an even lower contact angle, dewetting may become impossible.

3.1.2. Self-patterned deposition using PFOTS

Another method of achieving spin-on patterning for perovskites uses a hydrophobic layer made from silane, as demonstrated for octadecyltrichlorosilane (ODTS) by Lee et. al. [7]. Unlike the thin films produced by spincoating poly-TPD, silanes form a self-assembled monolayer (SAM) on glass substrates by chemically bonding to them. Additionally, they react violently with water and therefore require the use of a nitrogen glovebox for deposition.

Perfluorooctyltrichlorosilane (PFOTS) was used instead of ODTS, since it is currently in use at LNL with existing processing knowledge and facilities. Just like ODTS, PFOTS forms a hydrophobic SAM, which is typically used for anti-stiction coatings. Patterning the PFOTS SAM was first attempted using a top-down approach as shown for the ODTS SAM [7] using standard UV lithography, with RIE used for pattern transfer. However, this was found to be impossible due to the anti-stiction properties of the PFOTS SAM. No photoresist or thin film could be made to adhere to the surface during spincoating.

Since a top-down approach was not possible, a bottom-up approach was developed. Patterned PFOTS deposition was achieved by patterning photoresist on the sample be-

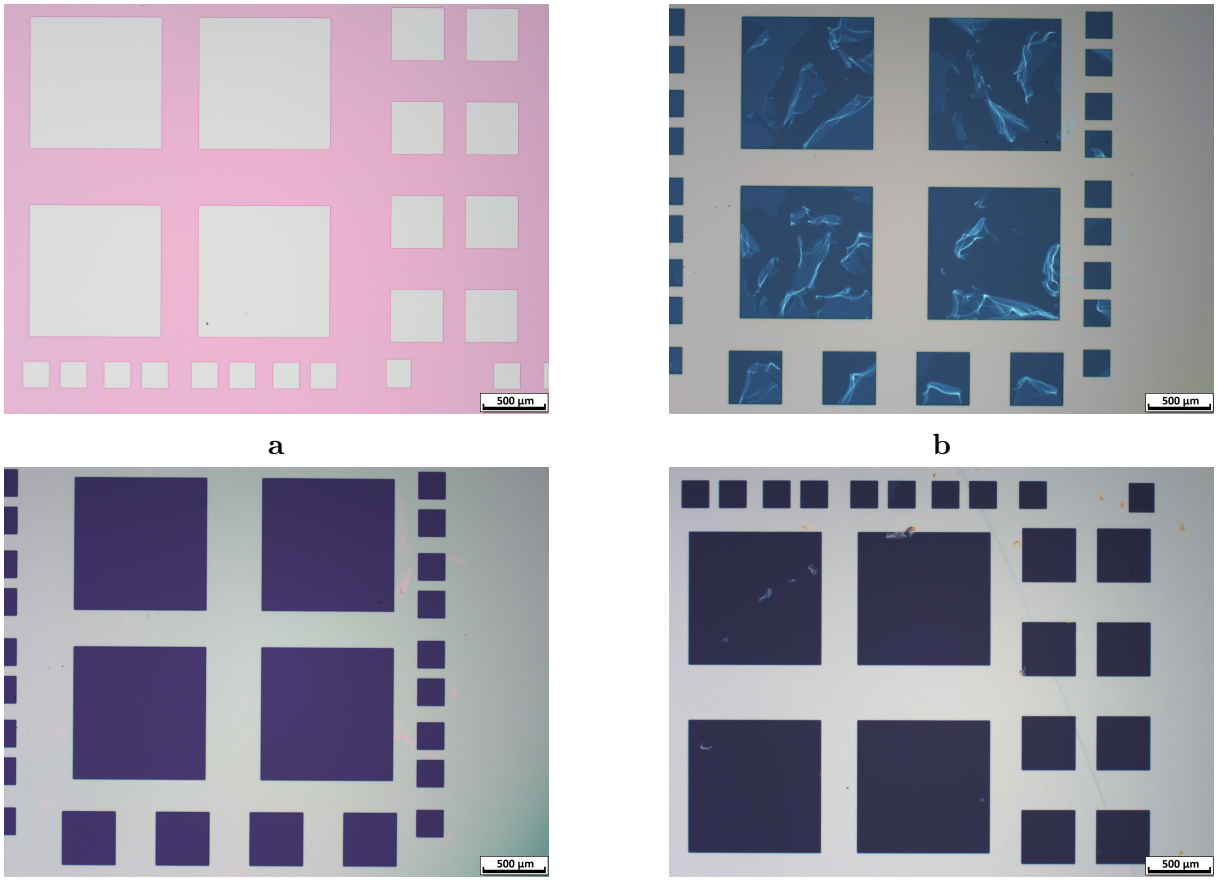

Figure 10: Optical microscope images of patterned poly-TPD films. a) Patterned AZ1505 photoresist on top of a poly-TPD layer. b) Sample after pattern transfer using chlorobenzene spin-drop casting. c) Sample after oxygen and argon etch to remove remaining poly-TPD. d) Patterned poly-TPD film after photoresist removal.

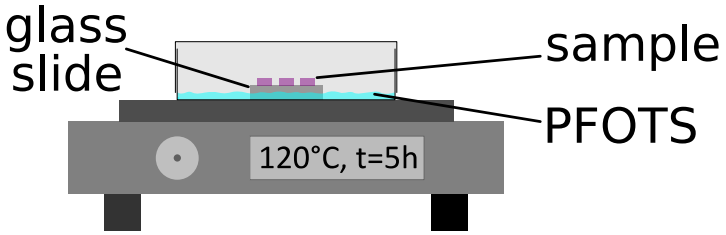

Figure 11: Setup used for PFOTS evaporation on substrates, with samples inside a sealed petri dish, elevated on glass slides from a pool of PFOTS. The programmable hot plate is used to facilitate thermal evaporation. The entire setup is located inside a nitrogen glovebox.

fore PFOTS deposition. During PFOTS, these areas are protected by the photoresist. As a result, they are left hydrophilic after the removal of the photoresist, whereas the unprotected areas are covered in hydrophobic PFOTS. To accomplish this, a first attempt was made using just AZ1505, spincoated at 3000 rpm and cured at 100 °C for 50 s. The photoresist was then exposed to 160 mJ cm^{-2} of UV light before development in AZ351B (diluted 1:5 in DI water) for 30 s, followed by a rinse in DI water.

Deposition of PFOTS layers was achieved by thermal evaporation in a nitrogen glovebox. The setup is as shown in Figure 11, with samples placed elevated on glass slides inside a covered petri dish on top of a programmable hot plate. Then $\approx$ 100 ml of PFOTS was injected through a hole in the top petri dish with a glass syringe, so that the liquid pooled at the bottom, below the elevated samples. The glass syringe is washed out with hexane before and after use to prevent PFOTS deposition. The hole is then covered up using a glass slide and the programmable hot plate is turned to 120 °C for 5 h. During this time the PFOTS evaporates thermally and builds up in the petri dish atmosphere where it then reacts with the sample surface to form a SAM. Although the standard process at LNL uses 180 °C, a lower temperature of 120 °C was used. This lower temperature still allows for PFOTS deposition but decreases the crosslinking which occurs in AZ1505 photoresist at temperatures above 140 °C.

Although the deposition was successful, the photoresist could not be removed, despite the decreased evaporation temperature. It is likely that the resist crosslinked due to the long evaporation time, while the PFOTS also deposited onto the resist layer, complicating removal. Even use of heated solvents in combination with a strong sonication were unable to remove the resist layer.

To facilitate a lift-off, a bilayer system consisting of AZ1505 photoresist and LOR0.7 was attempted. The LOR0.7 layer was selected, since it is unaffected by thermal crosslinking and is generally much more soluble. The LOR0.7 layer was spun on at 3000 rpm and cured at 150 °C for 4 min. After this, the AZ1505 photoresist was spun on at 4000 rpm, to create a thinner, easier-to-remove layer. Once the resist layer was patterned, PFOTS was evaporated onto the samples as described above. Afterwards, the resist layer could be removed by immersion in DMSO for 30 s, accompanied by ultrasonic bath if necessary.

The resulting patterned PFOTS layer is visible in optical pictures, although the contrast between the pristine and PFOTS covered areas is very low, since the SAM is very thin. With the naked eye, the PFOTS layer is much more clearly visible, due to the

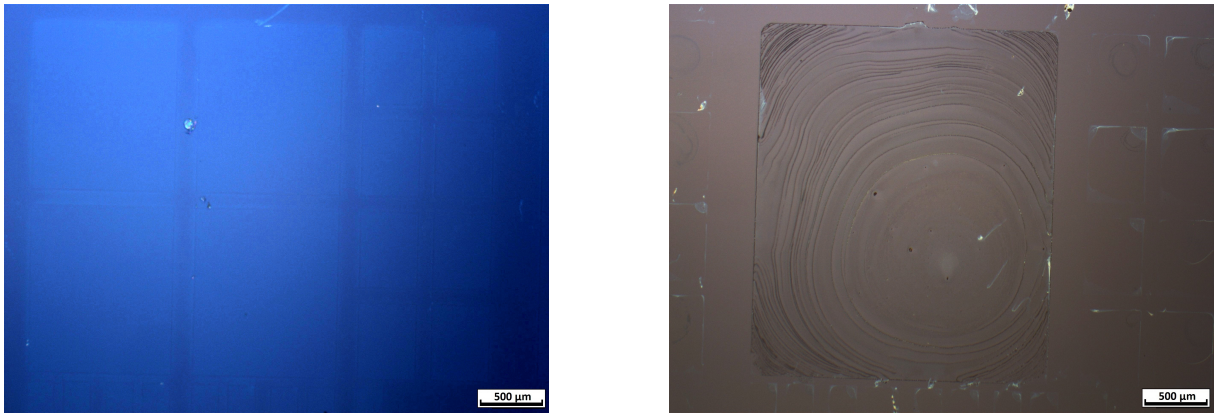

a **b**

Figure 12: Optical images of patterned PFOTS - SAM and patterned $CsPbBr_3$ perovskite deposited using patterned deposition on PFOTS -SAM. a) Optical microscope image of a patterned PFOTS monolayer on a plain Si/SiO_2 substrate. The contrast of the image was enhanced to make the SAM more perceivable. b) Patterned $CsPbBr_3$ film.

different reflectance. An image of a patterned area is shown in Figure 12a. The PFOTS SAM is absent in the lighter areas, in which perovskite should deposit during spincoating.

To verify that the dewetting and spin-on patterning was working for perovskite deposition, $CsPbBr_3$ was spun onto these samples. First, the $CsPbBr_3$ precursor was spun on at 1000 rpm for 60 s, which resulted in complete dewetting. Consequentially, the spin speed and time were lowered. Successful dewetting and precursor patterning was observed for very low spin speeds of 560 rpm. The samples were then heated at 100 °C for 10 min to allow the solvent to evaporate and the perovskite to crystallise. In Figure 12b it can be seen that the desired effect of patterned deposition was achieved, with perovskite selectively crystallising only in areas without PFOTS. However, the resulting pattern quality was poor, with devices commonly not filling up to the corners and exhibiting a significant amount of 3D crystal growth modes. The resolution of the pattern is low, with larger devices patterning more successfully than smaller devices.

At HZB, contact angle measurements were conducted using the triple-cation perovskite precursor. On plain substrates (hydrophilic) a contact angle of $\theta \approx 2°$ was measured, while on PFOTS the contact angle was $\beta = 83°$. These contact angles result in a critical liquid height $H_{crit} = 1133.2\,\mu m$ (s. Equation 2). This should allow for dewetting of the precursor at almost any spin speed, with higher speeds possibly running the risk of complete dewetting. Images of a sample with good device yield spincoated at HZB are shown in Figure 13. In Figure 13a, it can clearly be seen that the larger cells are patterned in much better quality when compared to the smaller cells on the left side of the image. The larger devices conform somewhat to the shape of the patterned PFOTS, with visible shrinkage and roughness to the device edges. The smaller devices displayed in Figure 13b still deposit in the designated areas, but crystallise out as droplets. It is likely that while there was enough liquid precursor to crystallise out in the defined shape, the precursor droplet contracted during crystallisation.

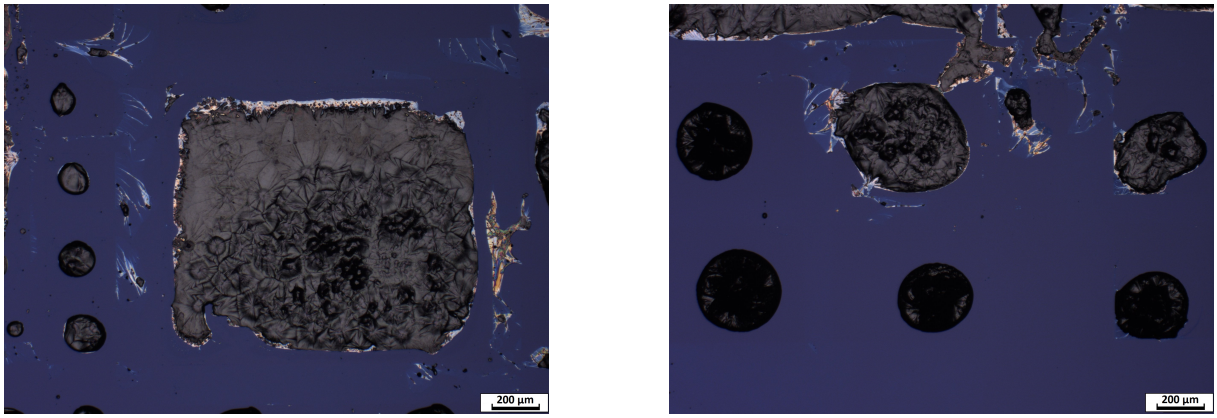

a **b**

Figure 13: Optical images of triple-cation perovskite deposited on patterned PFOTS samples at HZB. a) Image of large cell with small cells on the left. b) Image of smaller cells. It is clear that precursor contracted into a single drop during crystallisation.

3.2. Top-down patterning of perovskites

Following the unsuccessful attempts at patterned deposition, top-down patterning was attempted in order to create perovskite devices. To enable this, a compatible lithography system is required. An overview and discussion in regards to perovskite-compatibility of available resist systems is given in section 3.2.1. Next, a bilayer resist system based on a process published by Harwell et. al. [16] is discussed and processed.

3.2.1. Lithography on perovskites

To find a suitable lithographic system for use on perovskites, information was gathered on many established resist systems. A working top-down lithography (TDL) system is required for any top-down patterning method, but also for contacting patterned perovskite as the final processing step. Both UV and electron beam lithography, as well as positive and negative resist tones were considered, covering a significant amount of resist systems. In order for a resist system to be compatible with perovskite processing, the resist solvent, developer solution, and remover all need to be perovskite compatible. The processing chemicals for investigated resist systems are listed in Table 1, with the developer and remover chemicals taken to be those suggested by the manufacturer. It should be noted that for each resist system, alternative developers and remover chemicals exist. These were omitted in Table 1 for clarity.

By comparing the information in Table 1 with reported solvent solubility tests, the compatibility with perovskites can be deduced. Looking first at the resist solvent, it can be seen that most resists use a perovskite compatible solvent (PGMEA, chlorobenzene, anisole, mesitylene), with the exception of hydrogen silsesquioxane (HSQ) and SU-8, which are dissolved in methyl isobutyl ketone (MIBK) and cyclopentanone respectively. Both MIBK and cyclopentanone are known to dissolve perovskites. Moving on to developers, resists commonly use either tetramethylammonium hydroxide (TMAH) or an aqueous alkaline solution consisting of sodium hydroxide (NaOH) and sodium borate ($Na_2B_4O_7$).

Table 1: Processing chemicals for select commercial resist systems.

Information source	Resist name	Tone	Lithography method	Resist solvent	Recommended developer	Recommended remover
AllResist	AR-N 7000 series	negative	EBL (DUV possible)	PGMEA	TMAH : DI water	dibasic esters
Microresist	ma-N 2400 series	negative	EBL (DUV possible)	anisole cyclopentanone	aqueous alkaline	ethanol amine (aq)
Microresist	mr-EBL 6000	negative	EBL	anisole	PGMEA	ethanol amine (aq)
[21]	HSQ	negative	EBL	MIBK	TMAH : DI water	HF
MicroChemicals	AZ n-LOF 2000 series	negative	EBL (DUV possible)	PGMEA	TMAH : DI water	PGME oxalic acid
AllResist	AR-N 4300 series	negative	UV	PGMEA	TMAH : DI water	dibasic esters
AllResist	AR-N 4200 series	negative	UV	PGMEA	TMAH : DI water	dibasic esters
Microresist	ma-N 400 series	negative	UV	PGMEA anisole	TMAH : DI water	ethanol amine (aq)
Microresist	ma-N 1400 series	negative	UV	PGMEA anisole	TMAH : DI water	ethanol amine (aq)
Dow	cyclotene 4000 series	negative	UV	mesitylene	DPGDME : naphtha	piranha etch
[21]	SU-8	negative	UV	cyclopentanone	PGMEA	oxygen plasma
[21]	PMMA	positive	EBL (DUV possible)	anisole chlorobenzene	IPA : MIBK	acetone
[17]	PMMA	positive	EBL (DUV possible)	anisole chlorobenzene	chlorobenzene : hexane	chlorobenzene
[21]	ZEP520	positive	EBL	anisole	o-, m-, p- xylenes	dimethyl actemide
Microresist	mr-PosEBR	positive	EBL	anisole	amyl acetate	acetone
AllResist	AR-P 3100 series	positive	UV	PGMEA	aqueous alkaline	dibasic esters
AllResist	AR-P 5300 series	positive	UV	PGMEA	aqueous alkaline	dibasic esters
AllResist	ma-P 1200 series	positive	UV	PGMEA	aqueous alkaline	ethanol amine (aq)
MicroChemicals	AZ 1500 series	positive	UV	PGMEA	aqueous alkaline	ethanol amine (aq)
MicroChemicals	AZ 3000 series	positive	UV	PGMEA	aqueous alkaline	ethanol amine (aq)
Dow	S1800 series	positive	UV	PGMEA	TMAH : DI water	NMP
MicroChemicals	AZ 5200 series	image reversal	UV	PGMEA	TMAH : DI water	ethanol amine (aq)

These developers are generally thinned with DI water to tune development speed and resolution. Additionally, they are generally interchangeable, with most resists working with both TMAH developer (often advertised as metal-ion free) and aqueous alkaline developers. Both types of developers are not compatible with perovskite processing as both the active components as well as the DI water thinner dissolve perovskite.

Both SU-8 and Microresists mr-EBL 6000 use PGMEA (often referred to as SU-8 developer) as the developer, making their development perovskite-compatible. Although the standard MIBK: IPA 1:3 developer for poly(methyl methacrylate) (PMMA) is not compatible with perovskites, the chlorobenzene : hexane 1:3 mixture reported by Lin et. al. is [17]. The DS2100 developer for the cyclotene 4000 series, consisting of dipropylene glycol dimethyl ether (DPGDME) and naphtha was found to have no effect on triple-cation perovskite when a perovskite film was submerged for 5 min. The xylene developer used for ZEP520 would also be perovskite compatible, as xylenes can be employed as anti-solvents during perovskite processing [2, 22]. The amyl acetate developer used for Microresists mr-PosEBR resist has also been shown not to harm perovskites [23].

When looking at removers, it can instantly be noted that SU-8, HSQ, and cyclotene (photo-BCB) are not intended to be removed after patterning, requiring extremely aggressive chemicals and etching processes for removal, none of which are perovskite compatible. Similarly, the developers based on aqueous ethanol amine, N-methyl-2-pyrrolidone (NMP), acetone, and propylene glycol methyl ether (PGME) are incompatible. No information is available on the dibasic esters (dimethyl glutarate, dimethyl adipate, and dimethyl succinate) used in AllResists AR 300-76 remover. As with the developers, alternative removers exists, commonly acetone, NMP, or DMSO are reported as alternatives by the manufacturers.

In terms of a fully compatible process, only the modified PMMA process reported by Lin et. al. [17] is compatible with perovskites, using chlorobenzene and hexane to replace MIBK, IPA, and acetone. Additionally, the mr-Pos EBR resist by Microresist may also be compatible, as it shows good solubility in anisole according to Microresist. All other resist systems are not useable on perovskites in the form in which they are commonly processed.

However, while the PMMA process works on perovskites, it is unsuitable for patterning large areas of perovskite devices. Due to the positive tone, all non-device areas would have to be written in EBL. Processing for small samples with the high dosage requirements of PMMA requires an EBL machine with a beam current in the order of 20 nA. Full wafer-scale processing would be very time intensive but possible.

Although PMMA could also be processed using deep UV (DUV) lithography, PMMA also requires long exposure times for DUV processing (order of minutes). The resultant photodegradation is likely to significantly reduce device quality. Instead, PMMA is well suited for contact patterning as discussed in section 3.3. While no single resist system is suited for TDL patterning of perovskites, perovskite patterning was achieved using a combination of SU-8 and PMMA by Harwell et. al. [16] and successfully replicated as discussed in section 3.2.2.

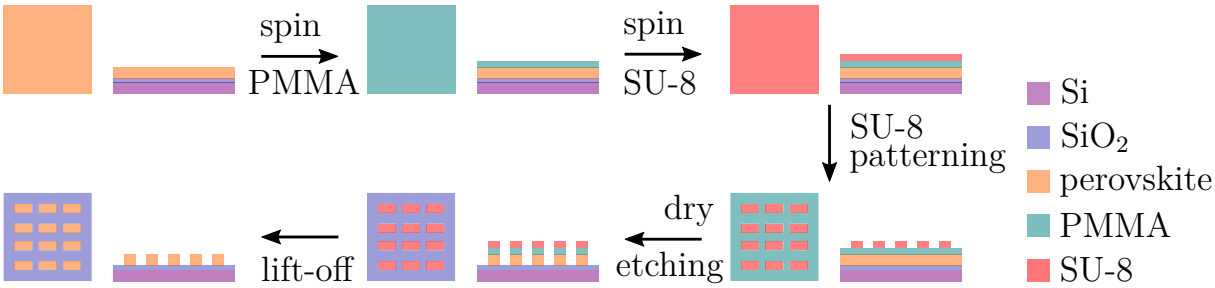

Figure 14: Processing scheme for patterning perovskites using a PMMA/SU-8 bilayer resist system.

3.2.2. Patterning of perovskite using a PMMA/SU-8 bilayer resist

As discussed in section 3.2.1, performing a standard TDL patterning process on perovskites fails due to the lack of a suitable lithography system. However, PMMA as a resist system is compatible with perovskites during both spincoating and removal. By combining a PMMA bottom layer with a top layer of SU-8, which is developed using perovskite compatible PGMEA, Harwell et. al. [16] successfully demonstrated the creation of patterned perovskite devices. In this process, the perovskite is coated with PMMA first, which serves as a buffer layer. To achieve patterning, SU-8 is spun onto the PMMA buffer layer, which protects the perovskite from the cyclopentanone solvent of the SU-8. The SU-8 is then patterned using standard UV lithography methods and developed using PGMEA. To transfer the pattern from the SU-8, dry RIE and ion beam etching (IBE) can be used. Afterwards, the remaining SU-8/PMMA stack on the perovskite devices can be removed by dissolving the PMMA in warm chlorobenzene. A schematic of the process is shown in Figure 14 and the experimental details and deviations from the Harwell process are discussed below.

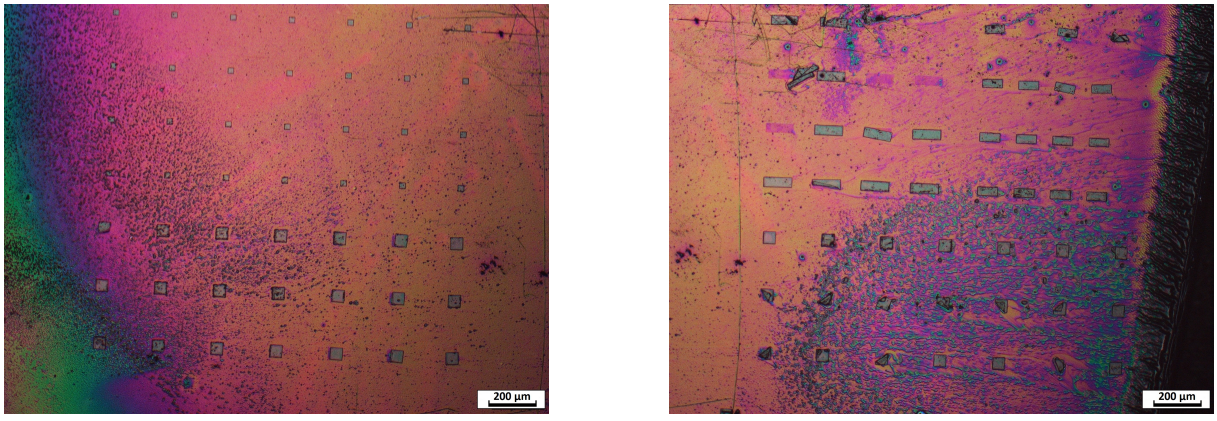

a **b**

Figure 15: Optical microscope images of patterned devices prior to milling and lift-off. The PMMA surface shows damage from SU-8 development and non-uniformity inherited from the surface roughness of the perovskite. a) Patterned 50 µm by 50 µm and 100 µm by 100 µm van-der-Pauw devices. b) Patterned transmission line devices (top half) and 100 µm by 100 µm van-der-Pauw devices (bottom half).

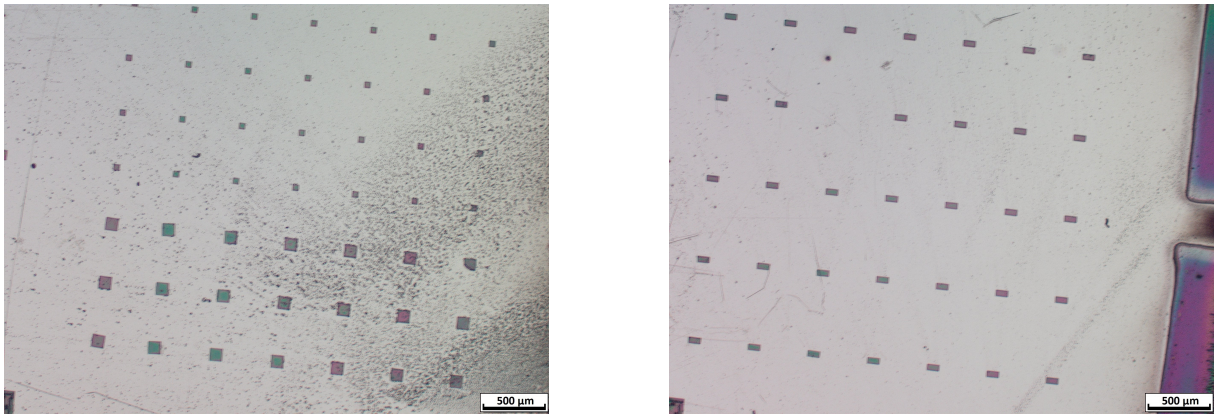

a **b**

Figure 16: Optical images of patterned SU-8 structures on top of PMMA/PSK after IBE. a) 50 µm by 50 µm and 100 µm by 100 µm van-der-Pauw devices. b) 100 µm by 50 µm Hall bar devices.

To create the samples, 950k A6 PMMA from MicroChem (now Kayaku Advanced Materials) was spun onto triple-cation perovskite on Si/SiO_2 substrates at 3000rpm before being cured at 120 °C on a hot plate for 10 min. An SU-8 solution equivalent in concentration to SU-8 2002 was created from SU-8 2050 and SU-8 thinner (cyclopentanone) as described in Appendix B. The SU-8 resist was spun onto the samples at 3000 rpm for 60 s before being cured at 95 °C for 120 s. This results in a resist thickness of 1.25 µm. The resist was then exposed to a 160 mJ cm^{-2} dose before a post-exposure bake at 95 °C for 120 s. Development then occurred in PGMEA for 30 s.

Optical images of the patterned SU-8 are shown in Figure 15. The SU-8 devices in darkish green can be seen on top of the PMMA layer. There is distinct surface roughness in the PMMA layer, which shows as wavy features. The pattern visible in the PMMA layer is inherited from the surface structure of the perovskite. This is evident when comparing the patterns in the PMMA to the pristine perovskite surface as pictured in Figure 8b. Additionally, the PMMA layer does not have consistent colouring, even away from the sample edge. This is likely a consequence of the SU-8 development, as PGMEA is also a solvent for PMMA, albeit a very poor one. Some SU-8 devices are missing, with a shadow visible in the PMMA, while others are tilted. The surface roughness of the PMMA combined with some PMMA dissolving in the PGMEA developer are likely contributing to the tilting and partial peeling of SU-8 structures, especially visible in Figure 15b. An attempt to include a 30 nm thick layer of gold as a diffusion barrier between the PMMA and SU-8 was made. This layer was intended to prevent PMMA dissolution during SU-8 development. Instead, the gold layer prevented the SU-8 from adhering to the sample and was thus omitted.

Next, the pattern was transferred to the perovskite layer using IBE for 1 h with a beam current of 20 nA and an extractor voltage of 500 V. During IBE the sample was placed at a 20°relative to the ion beam and rotated at 20 rpm to increase directionality of the etch. Compared to the process used by Harwell et. al. [16], the PMMA layer is not etched using RIE, but instead the entire PMMA/perovskite stack is milled. To allow this

difference in processing, the SU-8 layer was chosen to be thicker, providing a good margin of error in case of overmilling. The IBE was conducted using an argon milling tool at Chalmers Nanofabrication Laboratory in Gothenburg. The resulting samples are shown in Figure 16a and Figure 16b. They are overmilled, with the 100 nm SiO_2 layer of the substrate having been milled away, demonstrating that the milling time of 1 h is longer than required. Overmilling may also present a complication during contact processing, as a greater step between device edge and substrate may result in broken contact leads. Additionally, the contact pads would be connected conductively through Si. This is likely negligible due to the low doping of the wafer.

After IBE, it can be seen that the SU-8 resist is still present on top of the perovskite devices. Additionally, the perovskite surface roughness has visibly been transferred to the silicon substrate. To remove SU-8/PMMA resist layer, the sample was immersed in 60 °C warm chlorobenzene for a total of 60 min, with 70 s of sonication as the final step.

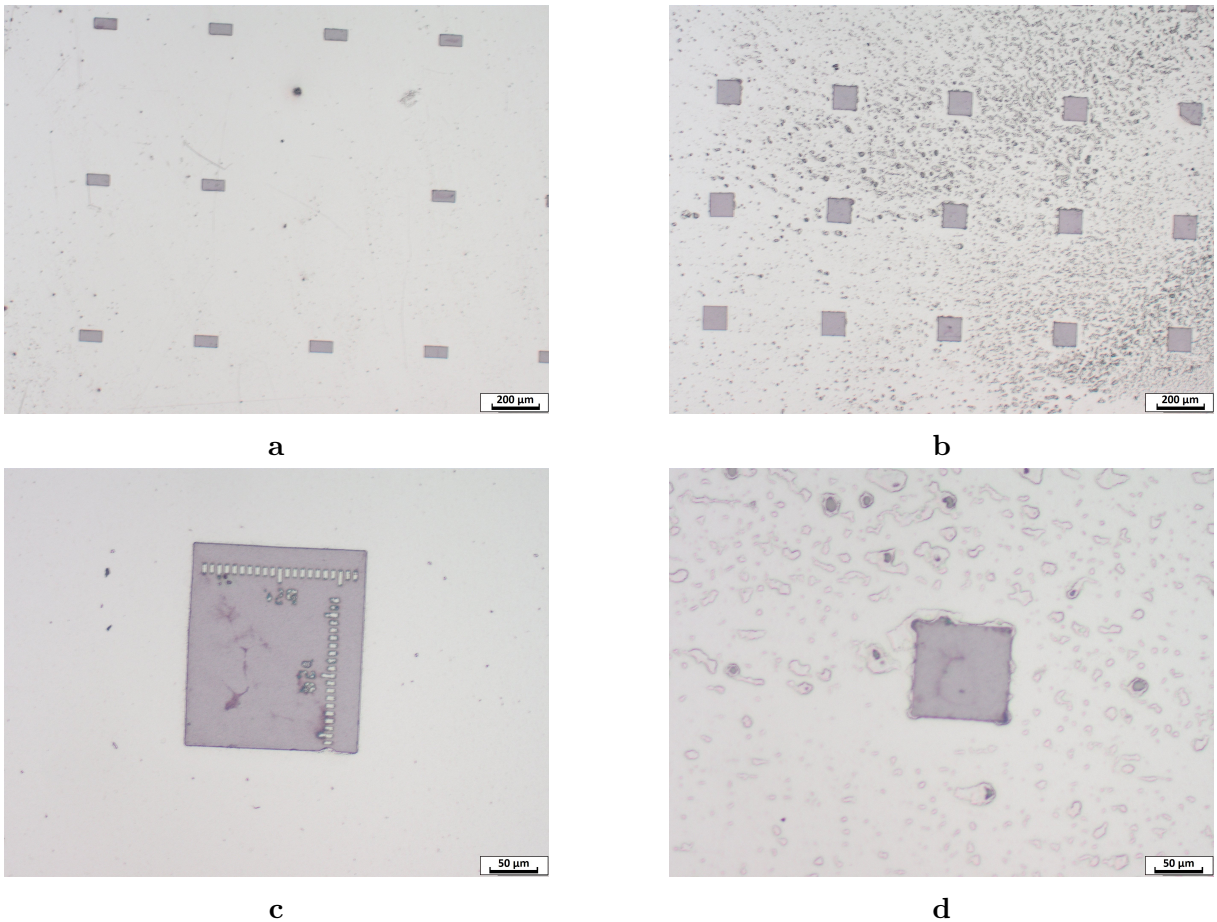

a **b**

c **d**

Figure 17: Optical images of milled perovskite devices after lift-off of the SU-8/PMMA resist system. a) 100 µm by 50 µm Hall bar structures. The missing device peeled off during SU-8 development. b) 100 µm by 100 µm van-der-Pauw devices. The pattern in the Si substrate is directly transferred from the perovskite surface during the milling. c) Alignment reticle after milling. The labelling is still legible and the 3 µm wide alignment ticks are visible. d) An individual 50 µm by 50 µm van-der-Pauw device.

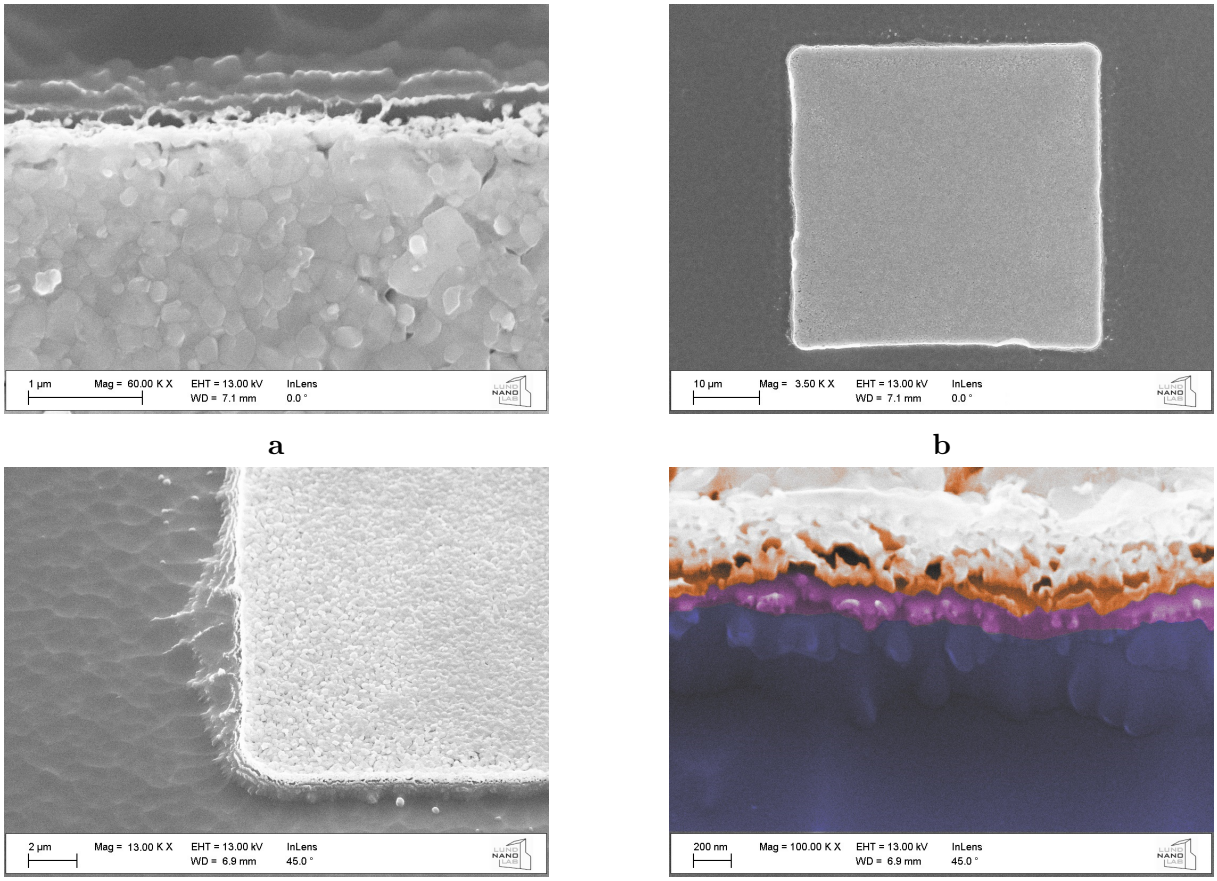

Figure 18: SEM images of milled perovskite devices. a) Edge of a device. b) 50 µm by 50 µm van-der-Pauw device imaged in SEM. It measures 44.74 µm (height) by 46.59 µm (width) in the SEM. c) Corner of a device viewed from an angle. d) Milled edge of a device viewed at an angle. The different layers of the device are highlighted using false colour, with the perovskite in orange, followed by purpleSiO_2 and blue Si.

Optical images of the devices can be seen in Figure 17. Both Figure 17a and Figure 17b show high device yield and quality. The small features on the scale of 3 µm still visible in Figure 17c show that the process can achieve micrometre resolution.

The patterned perovskite devices were also imaged using scanning electron microscopy (SEM) (s. Figure 18). The device shown in Figure 18b was designed to measure 50 µm by 50 µm but measures 44.74 µm (height) by 46.59 (width) in the SEM. When imaged at an angle (Figure 18c, Figure 18d) the structure of the device edge becomes more clear. It can be seen that the edge tapers instead of forming a clear step during the milling process. Figure 18d shows the layers of the device in false colour, with an orange perovskite layer, followed by a purple SiO_2 layer and blue Si layer.

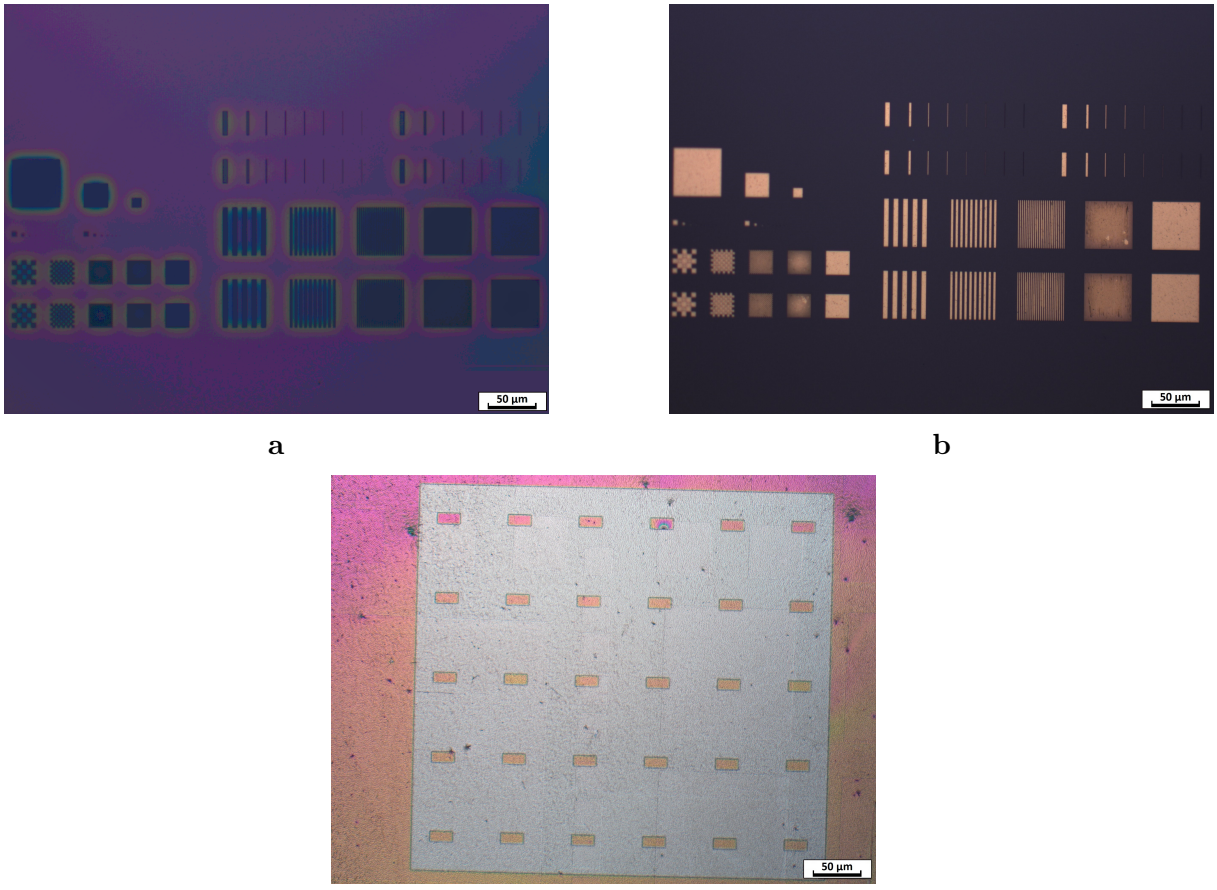

a **b**

c

Figure 19: Optical images of PMMA structures written on perovskite thin films. a) Dose test structure exposed at 400 µC cm^{-2} and developed using chlorobenzene:hexane 1:1 for 30 s. b) Dose test structure after evaporation of Ti/Au. Same structure as Figure 19a. c) Hallbar active areas written on perovskite using PMMA EBL.

3.3. Electrical contacts

To contact the perovskite devices, patterned contacts consisting of a carrier transport layer and metal need to deposited. To achieve this patterning EBL using a PMMA resist system was employed.

3.3.1. Electron beam lithography using PMMA on perovskites

To pattern electrical contacts, TDL is required. As discussed in section 3.2.1, only PMMA can be processed in a perovskite compatible fashion [17].

Commercial PMMA can be bought dissolved in anisole and chlorobenzene, both of which do not dissolve perovskite. Chlorobenzene thinned with hexane can be used as the developer. Lin et. al. [17] proposes a chlorobenzene:hexane ratio of 1:3. The resultant developer is not perfectly selective for exposed PMMA, since chlorobenzene will also dissolve unexposed PMMA. However, exposed PMMA will be dissolved more readily, which results in enough selectivity to allow for the development of structures. Lift-off and

removal of the PMMA is done by immersion in chlorobenzene, which can be warmed to 60 °C for faster dissolution.

To pattern contacts, a bilayer resist system consisting of 495k C4 PMMA bottom layer and a 950k A6 PMMA top layer was used. The numbers denote the chain length of the polymers in the PMMA, such that the 495k PMMA is lighter and more soluble than the 950k PMMA. This quicker dissolution creates an undercut during development, which facilitates lift-off of evaporated metal layers. Both resists were spun on at 4500 rpm and cured at 120 °C for 10 min on a hot plate.

A dose test was carried out to determine the correct exposure dose and development time for the resist stack. Using a Raith Voyager EBL (50 kV, high current mode, 60 µm aperture), the resist was exposed to doses between 50 µC cm^{-2} and 500 µC cm^{-2}. The resulting structures were developed for in chlorobenzene:hexane 1:1 developer for 30 s. A 1:1 ratio of chlorobenzene and hexane was used because the 1:3 ratio proposed by Lin et. al. [17] was found to be ineffective at developing any structures completely, even for time-spans exceeding 10 min. The minimum dose allowing for consistent development of all structures was determined to be 400 µC cm^{-2}. Images of the dose test structures after development and gold deposition are shown in Figure 19a and Figure 19b.

To confirm that the process worked on perovskite without destroying it, a Hall bar section from the final mask was written on a perovskite layer as seen in Figure 19c. Writing this section using PMMA EBL took 9 h using an exposure dose of 400 µC cm^{-2} and a beam current of 1.2 nA, even though it only represents a quarter of the active sample size. This demonstrates that while a perovskite patterning mask could be written using PMMA EBL, it requires a very high beam current.

3.3.2. Contact materials

A wide variety of contact materials are used in perovskite solar cell research, with the exact advantages and engineering of each still being a major focus of research [8, 9]. However, not all selective contact materials are suitable for the samples discussed here. Since the transport layers are being deposited on top of the perovskite, the deposition method must be perovskite compatible. Information on commonly employed transport layers was gathered in order to choose the best material for this project. The information is summarised in Table 2.

Many of these transport materials can be deposited on top of perovskite without damaging the perovskite. However, many require additional process development to function at their reported potential, which is outside the scope of this work. While spiro-OMeTAD is the most frequently used transport layer in perovskite solar cell research, it is almost never used as a pristine layer and only reaches its full potential through the use of dopants [8, 24]. This requires an avoidable degree of additional engineering and chemical processing. The PEDOT:PSS bipolymer is another popular choice, but due to its acidity it may speed up perovskite degradation [24]. Due to their solubility in chlorobenzene, poly(3-hexylthiophene) (P3HT), poly tri-arylamine (PTAA), phenyl-C61-butyric acid methyl ester (PCBM), and poly-TPD require a single deposition step for both transport layer and contact metal, as the PMMA lift-off occurs in chlorobenzene. Since all these transport materials are soluble in chlorobenzene, they need to be capped by the metal contact

Table 2: Properties and processing for common perovskite solar cell transport materials.

Material	Type	Valence band edge [eV]	Conduction band edge [eV]	Deposition method	Source
spiro-OMeTAD	HTL	-5.00 to -5.30	-2.05	spincoating (chlorobenzene)	[8, 24–26]
PEDOT: PSS	HTL	-5.00	-2.40	spincoating (toluene)	[8, 24, 27–30]
P3HT	HTL	-5.00 to -5.20	-2.80	spincoating (chlorobenzene)	[8, 24, 31]
PTAA	HTL	-5.14 to -5.25	-2.30	spincoating (chlorobenzene)	[8, 24]
poly-TPD	HTL	-5.20	-2.30	spincoating (chlorobenzene)	[6]
Nickel(II) oxide	HTL	-5.20 to 5.40	-1.80	sputtering	[8, 24, 32–34]
Copper(I) iodide	HTL	-5.10	-2.20	spincoating (chlorobenzene)	[8, 24, 35, 36]
Copper thiocyanate	HTL	-5.30	-1.50	spincoating (diethyl sulphide)	[8, 24, 37–41]
Graphene oxide	HTL	-4.90 to -5.20	-	spincoating (polar solvents)	[8, 24, 42]
PCBM	ETL	-6.00	-4.10	spincoating (chlorobenzene)	[9]
Buckminster fullerene	ETL	-6.20	-4.50	thermal evaporation	[9]
Titanium (IV) dioxide	ETL	-6.20 to -7.40	-3.90 to -4.10	reactive sputtering	[9]
Zinc (II) oxide	ETL	-7.60	-4.20	reactive sputtering	[9]
Tin (IV) dioxide	ETL	-6.20	-4.50	spincoating (DI water dispersion)	[9]

layer to protect them during the lift-off. This complicates an already difficult lift-off further, but these materials could potentially be used to contact the perovskite with a more mature process. Metal oxide based transport layers like TiO_2 are generally processed using thermal oxidation, which would cause thermal decomposition of the perovskite. Alternative low temperature deposition methods like reactive sputtering need to be calibrated tested when first introduced to a new machine. In contrast, copper thiocyanate (CuSCN) can be bought already in diethyl sulphide solution and deposited in a single spincoating step. Additionally, it does not dissolve in chlorobenzene or other perovskite processing solvents. This makes it a good choice for a first attempt at contacting perovskite with a PMMA EBL process. CuSCN is an HTL with a valence band edge at $-5.30\,\mathrm{eV}$ and a conduction band edge at $-1.50\,\mathrm{eV}$ [8, 24].

3.3.3. Contacting attempts using PMMA deep UV lithography

In order to address a high throughput solution, attempts were made to pattern contacts using DUV exposure of PMMA. Typically, PMMA is not used as a DUV resist because it requires long exposure times, in the order of minutes, due to the low absorption. Using the same resist processing (deposition, developement) as discussed in section 3.3.1, PMMA

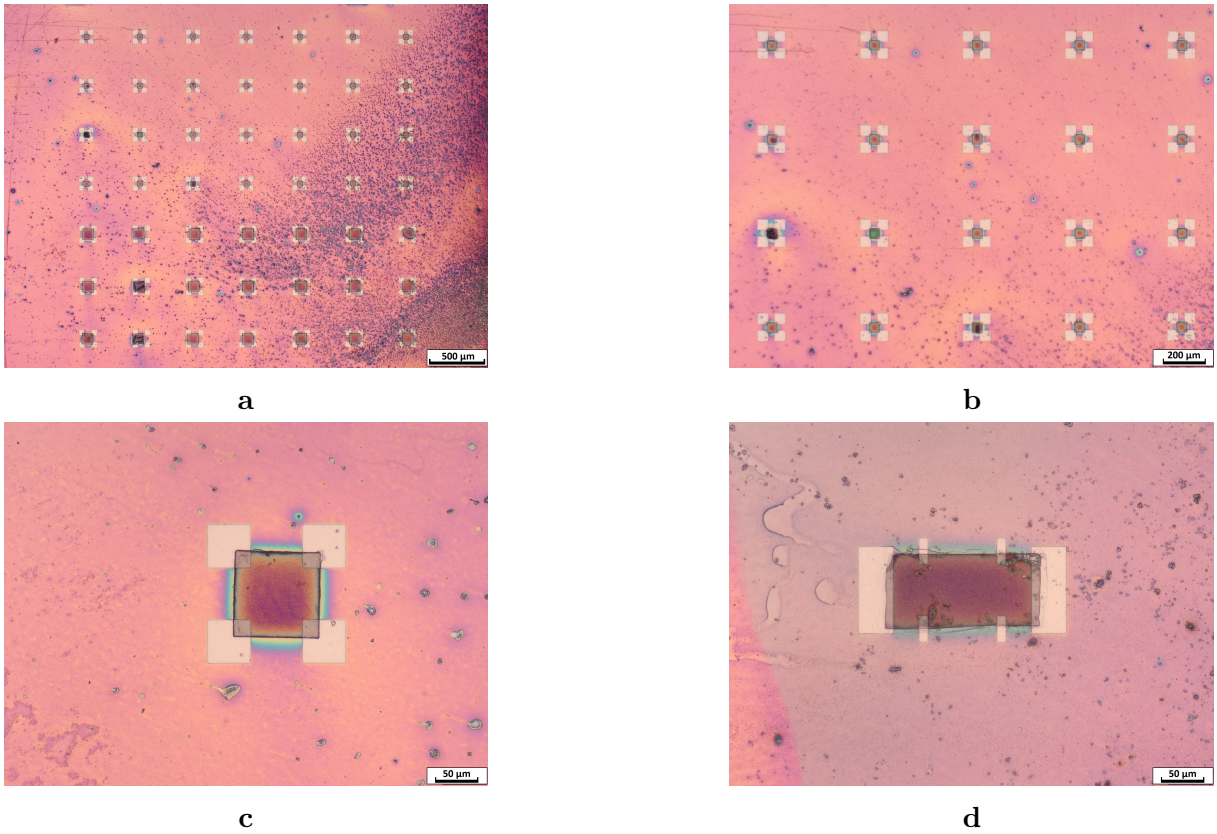

Figure 20: Optical images of patterned PMMA layer prior to CuSCN deposition. a) Array of van-der-Pauw devices. b) Array of van-der-Pauw devices. c) Van-der-Pauw transport layer. d) Hallbar transport layer patterned.

could successfully be patterned with a Karl Süss MJB4 DUV mask aligner using exposure times of 5 min. Images of patterned contact material structures can be seen in Figure 20.

The CuSCN transport layer was deposited via spincoating from diethyl sulphide solution at 3000 rpm, before being baked on a hot plate at 120 °C for 2 min to evaporate the solvent. The PMMA layer could then be lifted off by immersion in 60 °C warm chlorobenzene for 5 min followed by 20 s of ultrasonic bath. This resulted in a patterned CuSCN transport layer as shown in Figure 21. It can be seen that the patterning is imperfect, with the CuSCN either lifting off or remaining in unintended places. However, the resulting layer is still acceptable for processing into full devices. By improving the deposition of the CuSCN transport layer, as well as moving to the intended EBL patterning method, the quality of the films is likely to increase.

An attempt was also made to use DUV patterned PMMA to deposit the Ti/Au metal contact layer onto the CuSCN transport layer. However, no combination of resist thickness and metal layer thickness could be found that allowed for a successful lift-off. Therefore, no finished devices could be produced.

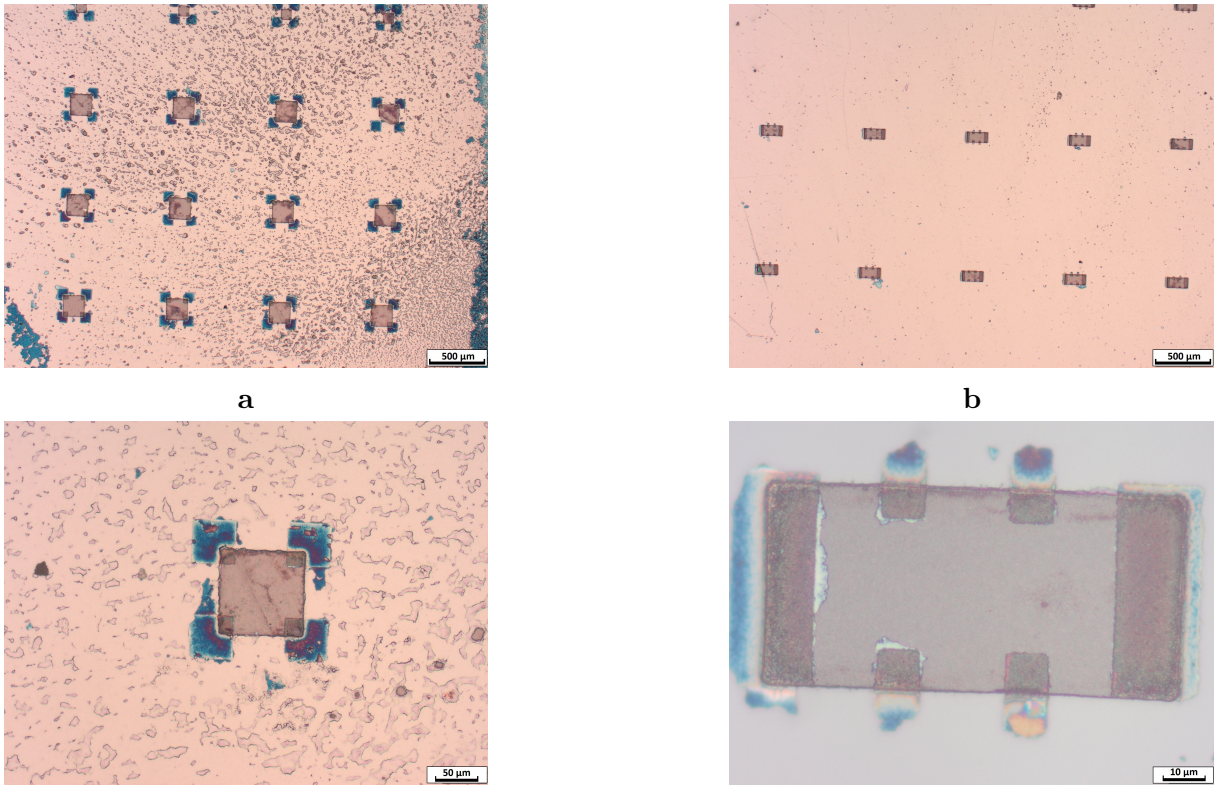

a **b**

c **d**

Figure 21: Optical images of patterned CuSCN layer on triple-cation perovskite devices. a) CuSCN transport layer patterned on 100 µm by 100 µm van-der-Pauw structures. b) CuSCN transport layer patterned on 50 µm by 100 µm Hallbars. c) CuSCN transport layer patterned onto a 100 µm by 100 µm van-der-Pauw structure. d) 50 µm by 100 µm hallbar with patterned CuSCN transport layer.

3.4. Photoluminescence measurements

PL spectra of perovskites are characteristic for the material composition. The PL spectrum of an as-deposited triple-cation perovskite film is shown in Figure 22a. Measurements of a device after processing are shown in Figure 22b. The decay in PL intensity and slight shift of peak position for consecutive measurements are a result of photodegradation in the perovskite due to the intensity of the laser excitation. By fitting curves to the data, it can be calculated that the PL spectra of pristine perovskite are centred around 781 nm. The PL spectrum of the processed perovskite is centred around 784 nm. This suggests that the perovskite has not significantly degraded during device processing.

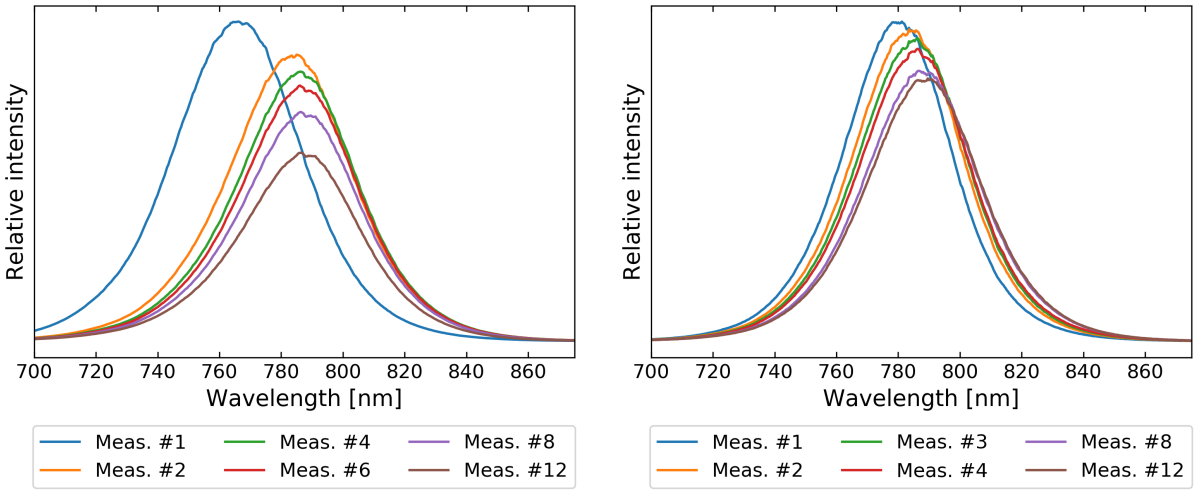

Figure 22: Photoluminescence spectra of [FAMACs]PbI_3 triple-cation perovskites before and after patterning. a) Photoluminescence spectrum of triple-cation perovskite before processing. b) Photoluminescence spectrum of a device patterned using the milling process described in section 3.2.2.

4. Discussion

4.1. Self-patterned deposition

Poly-TPD patterned spincoating was unsuccessful most likely due to insufficient hydrophobicity. While it may be possible to engineer the spincoating parameters in a way to allow patterned deposition using poly-TPD, it is clear that poly-TPD is does not create a sufficient hydrophobic effect.

When looking at the patterned perovskites produced using the PFOTS layer, the patterning quality is superior to the poly-TPD process. However, the definition or yield necessary to create devices suitable for measurement could not be achieved, since smaller devices crystallise out as droplets. When the solvent is evaporated off thermally, the precursor droplets inside the SiO_2 areas pull towards the centre of the hydrophilic area and then crystallise. This is more pronounced for smaller areas, but even in larger device

areas a distinct shrinking can be seen, with the perovskite edge being pulled inwards from the PFOTS edge.

In their work, Lee et. al. [7] used heated precursor and substrates to facilitate earlier crystallisation (i.e. during the spin coating process). This promotes the formation of seed crystals across the entire device area. During thermal curing, perovskite then grows from these seed crystals instead of the precursor pulling into a droplet.

The choice of substrate may also have contributed to the lack of success with patterned deposition. A silicon substrate with 100 nm thermal SiO_2 was used throughout all experiments, to provide electrical isolation of manufactured devices. Although the first batch of perovskite thin films could be produced on thermal SiO_2 without issue, later attempts showed complete dewetting on the thermal SiO_2 substrate even at slow spin-speeds. This indicates that perovskite deposition on thermal SiO_2 substrates is not as simple as initially thought and attempting patterned deposition with different substrates (e.g. plain Si, indium tin oxide) may be more successful. Alternatively, the SiO_2 surface could be roughened by chemical-mechanical polishing techniques in order to provide more nucleation sites for the perovskite during the spincoating. Care must be taken that this surface enhancement does not impact the performance of the PFOTS layer.

The advantage of the PFOTS layer over the poly-TPD layer is twofold. Firstly, the anti-stiction and hydrophobic properties of PFOTS are much more pronounced than those of poly-TPD. This allows for easier dewetting, often regardless of polarity of the solvent. This is clearly demonstrated by the inability to spincoat photoresist onto PFOTS. Secondly, the PFOTS SAM creates a visibly defect free surface. Both these factors contribute to the viability of the PFOTS process. Still, the PFOTS process is not without disadvantages, the most notable of which is the inability to easily remove the layer after depostion. As it is chemically bonded to the substrate, removal would require dry etching. This requires extra precautions to be taken so that the perovskite remains unharmed.

Overall, the results achieved with the PFOTS layer are promising, especially for devices requiring larger active areas. By optimising the patterning and spincoating procedure, it should be possible to achieve higher quality films with improved resolution. While the devices may initially be too large for the characterisation envisioned here, it is likely that the resolution limit can be pushed into the tens of micrometers.

The spincoating model used in this thesis provides good qualitative insight into the possibility of dewetting. However, neither contact angle nor any other interactions between surface and liquid play a role in modelling the spin curve. This means that results between different surfaces and liquids do not compare. For unpatterned films, this model calculates the exact same spincurve for both poly-TPD and PFOTS, which does not represent experimental reality. This is most clearly demonstrated by the AZ1505 photoresist, which could be used for top-down patterning of poly-TPD, but would not adhere to PFOTS films. Despite this, the model can still be used to evaluate the suitability of a hydrophobic and hydrophilic layer qualitatively, as well as providing intial paramters for the development of a spincoating process.

4.2. Top-down patterning

The top-down patterning process allows for high resolution patterning of the perovskite using compatible chemicals and only a single short lithographic step. By creating an appropriate mask, the process can be adapted to create different device structures. IBE is the ideal pattern transfer method for use with perovskites, as it uses chemically inert argon and works physically as opposed to chemically. In contrast, both reactive ion etching and wet etching work chemically. This can result in the perovskite only being partially removed, when one part of the perovskite is able to react with the etchant, while the other parts remains on the sample as a different salt [18]. With IBE, this possibility does not exist as argon is chemically inert and indiscriminately removes all atoms.

The fact that SU-8 remains on the sample even post-milling suggests a low milling rate for SU-8. This makes it an ideal resist for this process, as successful patterning can be achieved for a larger milling process window.

The top-down patterning process could be improved by the inclusion of a diffusion barrier layer between the PMMA and SU-8 resists, to prevent the peeling and tilting of SU-8 devices during development. While initial attempts using a gold spacer layer were unsuccessful, a different metal or sputtered oxide may work. It is important that this layer does not negatively affect the lift-off after the milling, as this is an already very sensitive step. By fine tuning the thicknesses of each resist layer, it should be possible to shorten the lift-off and milling time.

Compared to patterned deposition, top-down processing has some significant advantages. Firstly, the same perovskite layer could be patterned this way multiple times. Secondly, all layers involved in patterning can be removed, whereas SAMs such as PFOTS are difficult to remove from a sample, especially if unprotected perovskite is present. Thirdly, the achieving maximum resolution with the top-down process is much simpler. Whereas patterned deposition requires optimisation of the deposition parameters to achieve the highest resolution, the top-down patterning process is limited by the resolution of the lithography methods.

The top-down approach also builds on existing expertise in perovskite deposition. The same methods that are used to deposit high quality perovskite solar cells can be used to create high quality perovskite devices. In contrast, patterned deposition requires the development of a new deposition process. This means that top-down patterning currently allows for higher quality perovskite films. Moreover, the devices created using this method more accurately represent the material used for perovskite solar cells, which should make any obtained data more directly applicable to them.

4.3. Contact processing

Contact processing could not be fully demonstrated on actual devices, but the individual steps necessary were verified in the context of this work. Perovskite-friendly PMMA EBL processing was demonstrated, but could never be applied to milled devices due to a tool failure. While the DUV processing was only successful in depositing a transport layer, the full contact processing should be possible using EBL. Beyond this, EBL also offers the advantage of adapting contact designs to processing requirements. This is necessary

when moving to transport materials that are soluble in chlorobenzene,since it is necessary for these materials to deposit transport material and contact metal in a single lithography step.

5. Outlook

The natural continuation of the work is the fabrication and characterisation of finished devices. All individual process steps required to accomplish this were verified, most importantly the perovskite-compatible top-down patterning. The process for contact processing was demonstrated and partially executed on patterned perovskite devices, allowing for the creation of many different types of patterned perovskite devices.

Creating different types of semiconductor test devices than those created here can be done by developing upon the processing strategies presented in this work. By altering the lithography masks, different perovskite structures and contact structures can be produced. With small changes to the process, it should be possible to deposit transport material and contact metal in a single lithography step. This would enable the use of all top-deposition compatible contact materials, like spiro-OMeTAD, P3HT, PCBM, and many others. Investigating how contact quality and charge carrier properties differ between these transport materials would significantly advance the development of perovskite solar cells, providing important physical insights.

Improvement of the PFOTS process should be attempted. Here, it would be worth investigating different substrates, as the thermal oxide wafers were revealed to actually be a suboptimal substrate. Repeating the patterned deposition experiments conducted on SiO_2 covered wafers on plain Si wafers or chemically roughened Si/SiO_2 is therefore likely to reveal different results. For a different insulating substrate, glass covered with epitaxially grown Al_2O_3 should be investigated.

The patterning and contacting procedure presented in this work allows for the experimental investigation of perovskites in many different shapes and configurations. It also allows for the integration of perovskites with other technologies. Without a patterning and contacting scheme, it is not possible to create active device areas in the perovskite layer. This patterning and contacting scheme can therefore be used as a tool to enable researchers to create new types of devices and finally characterise perovskites in a manner that is consistent with established semiconductor processing techniques.

A. Dewetting model for water on poly-TPD

Using Equation 1 and Equation 2, the initial height is taken to be $h_0 = 0.5\,\text{mm}$, based on a liquid volume of 50 µl distributed on a $1\,\text{cm}^2$ substrate. Both L_{ox} and L_{phobic} were taken for the smallest features on the mask, since the critical height is lowest for the smallest features. The values are $L_{ox} = 200\,\mu\text{m}$ and $L_{phobic} = 90\,\mu\text{m}$. This results in $H_{crit} = 79.8\,\mu\text{m}$. The temporal evolution of liquid height for different spin speeds as well as the necessary H_{crit} to achieve dewetting are shown in Figure 23. It is obvious that dewetting should occur near instantaneously regardless of spinspeed, as a result of the large feature sizes (s. Equation 2), which should allow for easy spin-on patterning for these samples.

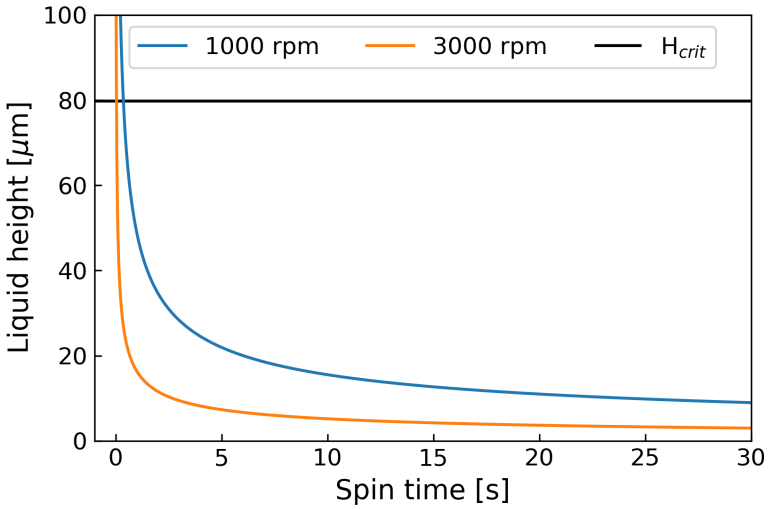

Figure 23: Model for dewetting of DI water on the prepared poly-TPD samples, calculated using Equation 1, with $H_{crit} = 62.9\,\mu\text{m}$ derived from Equation 2. Contact angles are as measured with hydrophilic contact angle $\theta = 49°$ and hydrophobic contact angle $\beta = 89°$. Initial height was taken to be $h_0 = 0.5\,\text{mm}$, with feature sizes $L_{ox} = 200\,\mu\text{m}$ and $L_{phobic} = 60\,\mu\text{m}$ for hydrophilic and hydrophobic features respectively, based on mask design.

B. Thinning SU-8 2050 resist to SU-8 2002 equivalent solution

SU-8 was thinned according to $m_{ini} = \frac{c_{2002}}{c_{2050}} m_{final}$, with m_{ini} initial mass of SU-8 2050 before thinning, c_{2002} and c_{2050} solid concentrations in the SU-8 2002 and 2050 resists respectively, and m_{final} the final mass of the SU-8 2002 solution. The final mass $m_{final} = 56.15\,\text{g}$ of SU-8 2002 was calculated using the mass density of SU-8 2002 given in the SU-8 processing guidelines by MicroChem for a final volume 50 ml. The solid concentrations $c_{2002} = 29.00\,\%$ and $c_{2050} = 71.65\,\%$ were also taken from the SU-8 processing guidelines. Using these values, a $m_{ini} = 22.73\,\text{g}$ (equivalent to 18.43 ml) was mixed with $\approx 32\,\text{ml}$ of cyclopentanone to achieve a SU-8 2002 equivalent resist solution. To verify the thinned resist, a spin curve was created by measuring the resist thickness with a profilometer for different spin speeds as shown in Figure 24. It is clear that the prepared SU-8 2002 solution is close to the commercial variant and should create a relatively thin SU-8 resist film.

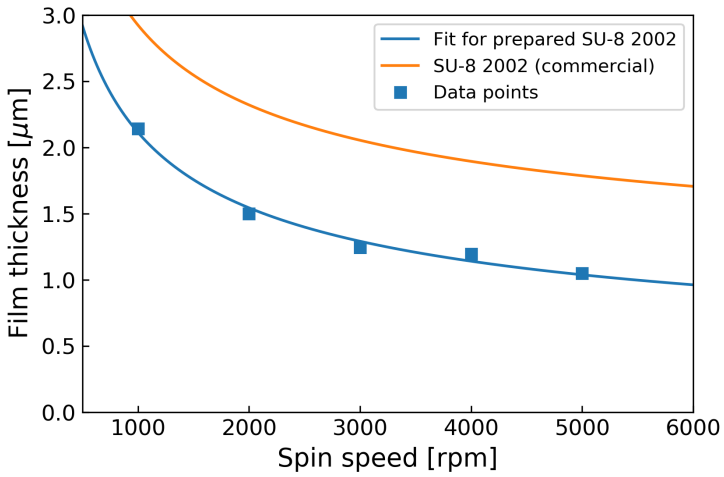

Figure 24: Spin curve of SU-8 2002 resist made by thinning down SU8 2050 with the spin-curve for commercial SU-8 2002 shown for comparison.

Acknowledgements

I would like to express my utmost gratitude to my supervisors Prof. Magnus Borgström and Dr. Michael Winters for the opportunity to perform this work and their guidance throughout the project. I greatly appreciate the freedom they gave me in exploring this topic. I especially want to thank Michael for sharing so much of his knowledge and experience with me. Moreover, the encouragement and support he provided whenever a process fell flat was fundamental to completing this work. I also want to thank him for travelling to Berlin to conduct the poly-TPD spincoating experiments, for producing the first batch of perovskite thin films there, and for travelling to Chalmers to conduct the milling procedures. All of these were essential to the project.

My thanks also go out to Dr. Eva Unger and Gopinath Paramasivam at HZB for their collaboration in this project. Specifically, I want to thank Gopi for spincoating the PFOTS samples, for providing me with triple-cation precursor, and for conducting contact angle measurements of precursor on PFOTS and thermal oxide samples.

Furthermore, I want to thank the staff at LNL for their instructions and for the opportunity to introduce perovskites into the lab. I am especially grateful to Natalia Volkova for lending her chemical expertise and for ensuring I got all the chemicals I needed, even when there was a bureaucratic mountain to climb. I also want to thank Dr. Bao Dang Ho and Dr. Jason Beech for helping me deposit the PFOTS and Dr. Reza Jafari Jam for training me on the Voyager EBL.

Lastly, I am thankful to my family and friends for supporting me throughout this entire project. Their support and encouragement has been more helpful than they can ever imagine.

References

1. Li, Z. *et al.* Scalable fabrication of perovskite solar cells. *Nature Reviews Materials* **3** (Mar. 2018).
2. Unger, E. L., Shargaieva, O., Braunger, S. & Docampo, P. in *Solar Energy Capture Materials* 153–192 (Royal Society of Chemistry, 2019).
3. Emery, K. *Best Research-Cell efficiencies* `https://www.nrel.gov/pv/cell-efficiency.html`.
4. Chen, Y. *et al.* Extended carrier lifetimes and diffusion in hybrid perovskites revealed by Hall effect and photoconductivity measurements. *Nature Communications* **7,** 12253. ISSN: 2041-1723. `https://doi.org/10.1038/ncomms12253` (2016).
5. Emslie, A. G., Bonner, F. T. & Peck, L. G. Flow of a Viscous Liquid on a Rotating Disk. *Journal of Applied Physics* **29,** 858–862 (May 1958).
6. Wu, J. *et al.* Pinhole-Free Hybrid Perovskite Film with Arbitrarily-Shaped Micro-Patterns for Functional Optoelectronic Devices. *Nano Letters* **17,** 3563–3569 (May 2017).
7. Lee, W. *et al.* High-Resolution Spin-on-Patterning of Perovskite Thin Films for a Multiplexed Image Sensor Array. *Advanced Materials* **29,** 1702902 (Aug. 2017).
8. Bakr, Z. H. *et al.* Advances in hole transport materials engineering for stable and efficient perovskite solar cells. *Nano Energy* **34,** 271–305 (Apr. 2017).
9. Lian, J., Lu, B., Niu, F., Zeng, P. & Zhan, X. Electron-Transport Materials in Perovskite Solar Cells. *Small Methods* **2,** 1800082 (July 2018).
10. J. H. Davies, D. *The Physics of Low-Dimensional Semiconductors* 460 pp. ISBN: 052148491X. `https://www.ebook.de/de/product/2783946/j_h_davies_davies_the_physics_of_low_dimensional_semiconductors.html` (Cambridge University Press, Apr. 18, 2009).
11. Deen, M. J. & Pascal, F. in *Springer Handbook of Electronic and Photonic Materials* 1–1 (Springer International Publishing, 2017).
12. Van der Pauw, L. J. A method of measuring specific resistivity and Hall effect of discs of arbitrary shape. *Philips Research Reports* (1958).
13. Al-Amri, A. M., Cheng, B. & He, J.-H. Perovskite Methylammonium Lead Trihalide Heterostructures: Progress and Challenges. *IEEE Transactions on Nanotechnology* **18,** 1–12 (2019).
14. Zhang, C. *et al.* Thermal stability of CsPbBr3 perovskite as revealed by in situ transmission electron microscopy. *APL Materials* **7,** 071110. `https://aip.scitation.org/doi/abs/10.1063/1.5108849` (2019).
15. Liu, L. *et al.* Photodegradation of Organometal Hybrid Perovskite Nanocrystals: Clarifying the Role of Oxygen by Single-Dot Photoluminescence. *The Journal of Physical Chemistry Letters* **10,** 864–869 (Feb. 2019).

16. Harwell, J. *et al.* Patterning Multicolor Hybrid Perovskite Films via Top-Down Lithography. *ACS Nano* **13,** 3823–3829 (Feb. 2019).

17. Lin, C.-H. *et al.* Orthogonal Lithography for Halide Perovskite Optoelectronic Nanodevices. *ACS Nano* (Dec. 2018).

18. Lyashenko, D., Perez, A. & Zakhidov, A. High-resolution patterning of organohalide lead perovskite pixels for photodetectors using orthogonal photolithography. *physica status solidi (a)* **214,** 1600302 (Oct. 2016).

19. Chu, Q.-Q. *et al.* Cost effective perovskite solar cells with a high efficiency and open-circuit voltage based on a perovskite-friendly carbon electrode. *Journal of Materials Chemistry A* **6,** 8271–8279 (2018).

20. Babayigit, A., Ethirajan, A., Muller, M. & Conings, B. Toxicity of organometal halide perovskite solar cells. *Nature Materials* **15,** 247–251 (Feb. 2016).

21. Chen, Y. Nanofabrication by electron beam lithography and its applications: A review. *Microelectronic Engineering* **135,** 57–72 (Mar. 2015).

22. Fang, F., Chen, J., Wu, G. & Chen, H. Highly efficient perovskite solar cells fabricated by simplified one-step deposition method with non-halogenated anti-solvents. *Organic Electronics* **59,** 330–336 (Aug. 2018).

23. Yang, F. *et al.* Dependence of Acetate-Based Antisolvents for High Humidity Fabrication of CH3NH3PbI3 Perovskite Devices in Ambient Atmosphere. *ACS Applied Materials & Interfaces* **10,** 16482–16489 (May 2018).

24. Pitchaiya, S. *et al.* A review on the classification of organic/inorganic/carbonaceous hole transporting materials for perovskite solar cell application. *Arabian Journal of Chemistry* (June 2018).

25. Wang, X. *et al.* High performance and stable perovskite solar cells using vanadic oxide as a dopant for spiro-OMeTAD. *Journal of Materials Chemistry A* **7,** 13256–13264 (2019).

26. Bi, D., Yang, L., Boschloo, G., Hagfeldt, A. & Johansson, E. M. J. Effect of Different Hole Transport Materials on Recombination in CH3NH3PbI3 Perovskite-Sensitized Mesoscopic Solar Cells. *The Journal of Physical Chemistry Letters* **4,** 1532–1536 (Apr. 2013).

27. Reza, K. M. *et al.* Tailored PEDOT:PSS hole transport layer for higher performance in perovskite solar cells: Enhancement of electrical and optical properties with improved morphology. *Journal of Energy Chemistry* **44,** 41–50 (May 2020).

28. Huang, D. *et al.* Perovskite solar cells with a DMSO-treated PEDOT:PSS hole transport layer exhibit higher photovoltaic performance and enhanced durability. *Nanoscale* **9,** 4236–4243 (2017).

29. Hu, L. *et al.* PEDOT:PSS monolayers to enhance the hole extraction and stability of perovskite solar cells. *Journal of Materials Chemistry A* **6,** 16583–16589 (2018).

30. Kostianovskii, V., Sanyoto, B. & Noh, Y.-Y. A facile way to pattern PEDOT:PSS film as an electrode for organic devices. *Organic Electronics* **44,** 99–105 (May 2017).

31. Giacomo, F. D. *et al.* High efficiency CH3NH3PbI(3-x)Clx perovskite solar cells with poly(3-hexylthiophene) hole transport layer. *Journal of Power Sources* **251,** 152–156 (Apr. 2014).

32. Hotový, I., Búc, D., Haščik, Š. & Nennewitz, O. Characterization of NiO thin films deposited by reactive sputtering. *Vacuum* **50,** 41–44 (May 1998).

33. Wang, K.-C. *et al.* p-type Mesoscopic Nickel Oxide/Organometallic Perovskite Heterojunction Solar Cells. *Scientific Reports* **4** (Apr. 2014).

34. Park, I. J. *et al.* New Hybrid Hole Extraction Layer of Perovskite Solar Cells with a Planar p–i–n Geometry. *The Journal of Physical Chemistry C* **119,** 27285–27290 (Nov. 2015).

35. Chen, W.-Y. *et al.* Low-cost solution-processed copper iodide as an alternative to PEDOT:PSS hole transport layer for efficient and stable inverted planar heterojunction perovskite solar cells. *Journal of Materials Chemistry A* **3,** 19353–19359 (2015).

36. Christians, J. A., Fung, R. C. M. & Kamat, P. V. An Inorganic Hole Conductor for Organo-Lead Halide Perovskite Solar Cells. Improved Hole Conductivity with Copper Iodide. *Journal of the American Chemical Society* **136,** 758–764 (Dec. 2013).

37. Mali, S. S., Patil, J. V., Kim, H., Luque, R. & Hong, C. K. Highly efficient thermally stable perovskite solar cells via Cs:NiO /CuSCN double-inorganic hole extraction layer interface engineering. *Materials Today* **26,** 8–18 (June 2019).

38. Jung, M. *et al.* Thermal Stability of CuSCN Hole Conductor-Based Perovskite Solar Cells. *ChemSusChem* **9,** 2592–2596 (Sept. 2016).

39. Madhavan, V. E. *et al.* Copper Thiocyanate Inorganic Hole-Transporting Material for High-Efficiency Perovskite Solar Cells. *ACS Energy Letters* **1,** 1112–1117 (Nov. 2016).

40. O'Regan, B., Lenzmann, F., Muis, R. & Wienke, J. A Solid-State Dye-Sensitized Solar Cell Fabricated with Pressure-Treated P25-TiO2and CuSCN: Analysis of Pore Filling and IV Characteristics. *Chemistry of Materials* **14,** 5023–5029 (Dec. 2002).

41. O'Regan, B. C. & Lenzmann, F. Charge Transport and Recombination in a Nanoscale Interpenetrating Network of n-Type and p-Type Semiconductors: Transient Photocurrent and Photovoltage Studies of TiO2/Dye/CuSCN Photovoltaic Cells. *The Journal of Physical Chemistry B* **108,** 4342–4350 (Apr. 2004).

42. Wu, Z. *et al.* Efficient planar heterojunction perovskite solar cells employing graphene oxide as hole conductor. *Nanoscale* **6,** 10505–10510 (2014).